

**Application of Cyclone Relative Approach and Ensemble Sensitivity Analysis to Better
Understand Extratropical Cyclone Errors in Operational Models and Ensembles**

A Thesis Presented

by

Xinxia Song

to

The Graduate School

in Partial Fulfillment of the

Requirements

for the Degree of

Master of Science

In

Marine and Atmospheric Science

Stony Brook University

August 2017

Stony Brook University

The Graduate School

Xinxia Song

We, the thesis committee for the above candidate for the
Master of Science degree, hereby recommend
acceptance of this thesis.

Dr. Brian A. Colle, Thesis Advisor

Professor

School of Marine and Atmospheric Sciences

Dr. Edmund K. M. Chang, Thesis Reader

Professor

School of Marine and Atmospheric Sciences

Dr. Michael M. French, Thesis Reader

Assistant Professor

School of Marine and Atmospheric Sciences

This thesis is accepted by the Graduate School

Charles Taber

Dean of the Graduate School

Abstract of the Thesis

Application of Cyclone Relative Approach and Ensemble Sensitivity Analysis to Better Understand Extratropical Cyclone Errors in Operational Models and Ensembles

by

Xinxia Song

Master of Science

in

Marine and Atmospheric Science

Stony Brook University

2017

A cyclone relative approach and an ensemble sensitivity analysis (ESA) were applied to explore some of the possible reasons for extratropical cyclone center mean sea level pressure errors. For the cyclone relative approach, data were extracted within a box region and saved every 6 hours. GEFS (Global Ensemble Forecast System) control member and ensemble members forecast data were utilized in this research.

Around the cyclone, errors in fields such as mean sea level pressure and precipitation rapidly increase from day 4 to day 5, and the errors of all fields examined are consistent with the overpredicted and underpredicted cyclones. For example, for an overforecast cyclone, it has more intense PV (potential vorticity) at 320K, a stronger temperature gradient on 925 hPa, and greater simulated precipitation than observed, while the underpredicted cyclones have the opposite results. The day 3 precipitation errors and 925 hPa temperature gradient errors are relatively large before the cyclone errors develop, thus suggesting that latent heat and dry dynamics could contribute to cyclogenesis intensity errors.

ESA accompanied with cyclone relative approach implies that moisture may contribute to the cyclogenesis error at an initial stage of cyclone development. There are also hints of upstream errors growing and moving in from ESA cases. A possible explanation for underpredicted cyclones might be that less moisture on the warm side of cyclones leads to a weaker upper tropospheric latent heat release, and hence a less amplified PV field, and a

weaker cyclone. In addition, a weaker temperature gradient at 925 hPa could also cause a weaker cyclone.

Table of Contents

List of Figures.....	vii
Acknowledgments.....	xi
Chapter I: Introduction.....	1
a. Background.....	1
b. Motivation.....	8
Chapter II: Data and Methods.....	12
a. Data.....	12
b. Tracking and matching methods.....	13
c. Cyclone relative approach.....	14
d. “Box” method.....	14
e. Case selection.....	15
f. Ensemble sensitivity analysis (ESA) method.....	15
Chapter III: Cyclone relative approach results.....	21
a. Mean sea level pressure results.....	21
b. PV (potential vorticity) at 320K theta level results.....	22
c. 925 hPa temperature gradient results.....	23
d. Precipitation results.....	24
Chapter IV: Ensemble sensitivity single case studies.....	37
a. 30 January 2010 overpredicted case.....	37
b. 07 October 2009 underpredicted case.....	39
c. 12 October 2011 underpredicted case.....	42

Chapter V: Conclusions.....	57
References.....	61

List of Figures

Fig 1. (left, a) 2007-2015 cyclone density errors (hPa: cyclone forecast errors per degree square per cyclone) plot for medium range forecast (72-120 h) spatial distribution in 20 GEFS ensemble members. (right, b) Medium range forecast (72-144 h) spatial distribution of cyclone intensity mean error (hPa) for NCEP GEFS ensemble members. Dashed contoured values indicate the standard deviation (hPa) for each grid point. (Korfe 2016).....	11
Figure 2. 2007-2015 cyclone density (cyclone numbers per degree square) plot for large (exceed one standard deviation threshold) negative (right) and large positive (left) error cases for underdeepening situation and overdeepening situation in 20 GEFS ensemble members for hour 102-120.....	11
Figure 3. Locations where cyclones are tracked and the 2007-2015 cyclone density (cyclone numbers per degree square) distribution of all time step tracks of cyclones which have large positive and negative errors during hour 108 - 120 in 20 GEFS ensemble members.....	18
Figure 4. (Left) the mean sea level pressure (hPa, shaded), the black box shows the cyclone relative domain and red x shows the cyclone center. (Right) the extracted cyclone relative field.....	18
Figure 5. Example of box method area.....	19
Figure 6. GEFS error distribution. The mean is 0.1hPa, and standard deviation is 8.1hPa. All cyclone cases of GEFS control member and all time steps are included.....	19
Figure 7. projection of y on x in 2D space.....	19
Figure 8. Yellow small box area is projection coefficient calculation area. Larger domain is ESA calculation area.....	20
Figure 9. GEFS control member mean sea level pressure relative error (shaded; model minus analysis) and model forecast (contoured) for overdeepened cases (left) and underdeepened cases (right) at hour 54-72 (top), 78-96 (middle) and 102-120 (bottom).....	27

Figure 10. GEFS control member mean sea level pressure (hPa) overdeepened cases error minus underdeepened cases error at hour 54-72 (top), 78-96 (middle) and 102-120 (bottom).....	28
Figure 11. GEFS control member PV (potential vorticity) at 320K theta level relative error (shaded; model minus analysis) and model forecast (contoured) for overdeepened cases (left) and underdeepened cases (right) at hour 54-72 (top), 78-96 (middle) and 102-120 (bottom).....	29
Figure 12. GEFS control member potential vorticity at 320K (PVU) overdeepened cases error minus underdeepened cases error at hour 54-72 (top), 78-96 (middle) and 102-120 (bottom).....	30
Figure 13. GEFS control member 925 hPa temperature gradient relative error (shaded; model minus analysis) and model forecast (contoured) for overdeepened cases (left) and underdeepened cases (right) at hour 54-72 (top), 78-96 (middle) and 102-120 (bottom).....	31
Figure 14. GEFS control member temperature gradient at 925 hPa ($\text{K}/10^3\text{m}$) overdeepened cases error minus underdeepened cases error at hour 54-72 (top), 78-96 (middle) and 102-120 (bottom).....	32
Figure 15. GEFS control member 925 hPa temperature gradient box area (shown previously) daily averaged errors for overdeepend cases (left) and underdeepend cases (right) distributions at day 3 (top), day 4 (middle) and day 5 (bottom). $h=1$ means the mean of this distribution is significantly different from 0 and $h=0$ means the opposite.....	33
Figure 16. GEFS control member precipitation relative error (shaded; model minus analysis) and model forecast (contoured) for overdeepened cases (left) and underdeepened cases (right) at day 3 (top), day 4 (middle) and day 5 (bottom).....	34
Figure 17. GEFS control member precipitation (mm/day) overdeepened cases error minus underdeepened cases error at day3 (top), day4 (middle) and day5 (bottom).....	35
Figure 18. GEFS control member precipitation box area (shown previously) daily averaged errors for overdeepend cases (left) and underdeepend cases (right) distributions at day 3 (top),	

day 4 (middle) and day 5 (bottom). h=1 means the mean of this distribution is significantly different from 0 and h=0 means the opposite.....	36
Figure 19. 20100130 (overpredicted case) daily ensemble sensitivity (shades) and ensemble mean mean sea level pressure (contours). The green line area has significance over 95%.....	45
Figure 20. 20100130 (overpredicted case) daily ensemble sensitivity (shades) and ensemble mean geopotential height at 700hPa (contours). The green line area has significance over 95%.....	46
Figure 21. 20100130 (overpredicted case) daily ensemble sensitivity (shades) and ensemble mean total column water (contours). The green line area has significance over 95%.....	47
Figure 22. 20091007 (underpredicted case) daily ensemble sensitivity (shades) and ensemble mean mean sea level pressure (contours). The green line area has significance over 95%.....	48
Figure 23. 20091007 (underpredicted case) daily bad member minus good member's difference (shades) and ensemble mean mean sea level pressure (contours).....	49
Figure 24. 20091007 (underpredicted case) daily ensemble sensitivity (shades) and ensemble mean geopotential height at 700hPa (contours). The green line area has significance over 95%.....	50
Figure 25. 20091007 (underpredicted case) daily bad member minus good member's difference (shades) and ensemble mean geopotential height at 700 hPa (contours).....	51
Figure 26. 20091007 (underpredicted case) daily ensemble sensitivity (shades) and ensemble mean total column water (contours). The green line area has significance over 95%.....	52
Figure 27. 20091007 (underpredicted case) daily bad member minus good member's difference (shades) and ensemble mean total column water (contours).....	53
Figure 28. 20111012 (underpredicted case) daily ensemble sensitivity (shades) and ensemble mean mean sea level pressure (contours). The green line area has significance over 95%.....	54
Figure 29. 20111012 (underpredicted case) daily ensemble sensitivity (shades) and ensemble mean geopotential height at 700hPa (contours). The green line area has significance over 95%.....	55

Figure 30. 20111012 (underpredicted case) daily ensemble sensitivity (shades) and ensemble mean total columnwater (contours). The green line area has significance over 95%.....56

Acknowledgements

Financial support for this work was provided through NOAA.

I sincerely want to thank Dr. Brian Colle for his advice and expertise and challenging me to become a better scientist and a professional. His dedication to the scientific community is unparalleled.

Special thanks go to the SOMAS faculty and colleagues, particularly Haiyang Yu, Yang Zhou for their friendship and camaraderie during my time here at Stony Brook University.

Chapter I: Introduction

a. Background

Extreme weather takes many lives, causes untold human hardship, and results in huge economic losses (Karl and Easterling 1999). Extratropical storms often result in heavy precipitation, strong winds, inland flooding (Easterling et al. 2000), and coastal flooding (Colle et al. 2008). Goodwin (2003) found that poor driving conditions during winter storms result in nearly 3,000 deaths and 1.4 million accidents each year across the U.S. It is important to determine numerical weather prediction (NWP) models' ability to forecast hazardous weather in order to improve these models. Research aiming at increasing the short and medium range forecast accuracy of extratropical cyclones will improve public safety.

Some storms are well forecast such as the Superstorm of March 1993 along the U.S. east coast (Uccellini et al. 1995). This cyclone rapidly developed along the east coast on 8-9 Feb 2013, resulted in snow reports of 0.48 - 1.01 m along the seaboard areas of New York and Connecticut (Picca et al. 2014). However, this cyclone was relatively well forecast 2-3 days beforehand using the key information supported by European Center for Medium Range Forecasts (ECMWF) high-resolution model to investigate cyclone development 6 days in

advance (Grumm et al. 2014). Other events are poorly forecast, such as the 25 January 2000 cyclone event moving along the North Carolina coast, where the operational Eta Model forecast model missed most of the precipitation over land and all over the Atlantic coast, showing a significant forecast uncertainty from the medium range (days 4-6) to the short range (day 1-3) (Zhang et al. 2002).

The atmosphere is a chaotic system (Lorenz 1963), and the estimated predictability limit is approximately two weeks (e.g. Lorenz 1982). In early years, forecast errors due to models dominated the total error growth. Now that, however, models are becoming more sophisticated, thus smaller errors that grow into larger errors dominate forecast uncertainty (Toth et al. 1997). To help move operational forecasts more towards probabilistic forecasts, ensemble weather forecasting was first introduced by Epstein (1969) and proposed by Leith (1974). However, the ensemble strategy will only work if the model has skills and the ensemble is calibrated. Ensembles have been used at operational centers such as the National Centers for Environmental Prediction (NCEP) and the ECMWF (Buizza et al. 1993; Molteni et al. 1996) for at least two decades. Ensembles are a collection of possible forecast scenarios from models that are equally likely and that will hopefully represent the true state of the

atmosphere (Toth et al., 1997). An estimation of the probability density function of forecast states can be obtained by integrating an ensemble of forecasts with each starting from slightly different initial conditions (Leith 1974). Numerous studies have demonstrated the benefits of using ensembles in forecasting. Zhu et al. (2002) found that a wide range of potential users could benefit from an ensemble rather than from a single deterministic forecast, thus offering more economic value. Stensrud et al. (1999) indicated that the loss of cyclone location accuracy from a reduction in model resolution can be recovered by using an ensemble approach. Froude et al. (2007) illustrated that ensemble prediction of extratropical cyclones can provide additional information to that obtained from a deterministic forecast. One particular advantage of ensemble forecasting highlighted was the measure of risk that can be provided via probabilities. Johnson and Swinbank (2009) showed a simple combination of ensembles from different operational centers can give a significant improvement in the predictive skill.

Many ensembles have been verified in various regions, but few ensemble studies target specific types of weather phenomena. Charles and Colle (2009) verified the position and strength of extratropical cyclones for six regions around North America and the adjacent

oceans within the Short Range Ensemble Forecast (SREF) system during the 2004-2007 cool seasons (October - March). The 15-member SREF mean performs a better overall forecast than various subgroups within it for cyclone position and cyclone central pressure along the East Coast and the western Atlantic.

Meanwhile, featured relative approaches have been used to better understand model error and processes associated with specific weather phenomena. Using cyclone relative composites, Bengtsson et al. (2009) investigated how extratropical cyclones may change in a warmer climate. They used cyclone-relative composite of the same 100 most intense storms horizontal structure in the model at different life cycle stages. Their study exhibited that highest precipitation happens ahead of the center in the region of strong ascent and on average, 15 h after the time of maximum intensification. Chang and Song (2006) used a cyclone relative field technique to study the precipitation from extratropical cyclones and found over the western North Pacific that there is more precipitation to the northeast of cyclone centers during fall than in winter and less precipitation southwest of cyclone centers in spring than in winter. Naud et al. (2012) applied cyclone centered composites and found that both Northern and Southern Hemispheres have similar cloud and precipitation

distributions during the early stages of a cyclone life cycle. When cyclones developed into a mature stage, both cloudiness and precipitation at the warm front increase in the northern Hemisphere but decrease in southern Hemisphere. Cloudiness in southern Hemisphere storms is more sensible to variations in atmospheric water vapor content, and therefore variations in surface temperature. Field and Wood (2007) also used the cyclone relative field technique on a total of 1500 cyclones from 4 mid-latitude oceanic regions and found for a given strength and water vapor content, cyclones are broadly similar in different geographical locations. Their study showed that if atmospheric moisture is doubled, a 50% increase in cyclone strength is detected.

Diabatic processes can play an important role resulting in model cyclone errors. Gray et al. (2014) analyzed tropopause-level Rossby wave ridges and troughs and found that diabatic processes can change Rossby wave structure, which can induce errors from model processes propagating downstream across the North Atlantic. Melhauser and Zhang (2012) concluded that small-scale errors in short term forecasts (0-36h) result from moist processes at scales < 100 km that rapidly grow upscale due to the nonlinearity inherent in the moist processes. Sun and Zhang (2016) found that in a moist environment with strong convective instability, rapid

upscale growth from moist convection leads to the forecast error being increasingly less sensitive to the scale and amplitude of the initial perturbations when the initial-error amplitude is getting smaller. Forecast uncertainties in the midlatitudes in recent NWP models have been found to be linked to errors in the Rossby wave pattern. Davies and Didone (2013) indicated that poorly predicted warm conveyor belts contribute a lot to altering Rossby waves propagating along the waveguide, which alters the development of the flow downstream from the warm conveyor belt. Rodwell et al. (2013) found that prediction errors can result from failures of numerical models to accurately capture diabatic ridge amplification, which result from misforecast of enhanced mesoscale convective systems activity with convective forecast busts over Europe. Chagnon et al. (2013) proposed that exchanges of heat due to diabatic processes in clouds modify flow structures like warm and cold conveyor belt and dry intrusions.

The ensemble sensitivity method as applied to an ensemble forecast can also be used to study the relationship between cyclone relative errors with surrounding atmospheric structure. Zheng et al. (2013) applied ESA to a U.S. East Coast snowstorm, which effectively relates the correlation between leading empirical orthogonal functions (EOFs) with cyclone intensity

and track uncertainty separately. They found for the 5.5-day forecast, the amplitude uncertainty of the ensemble is mainly related to the development of upstream trough and ridge systems crossing the northeastern North Pacific and central United States 108 h prior to the event. Chang et al. (2013) used ESA to study the evolution of two extreme extratropical cyclones over the Pacific applying the correlation between principal components (PCs) of the leading EOFs and sea level pressure. Their results show that coherent sensitivity patterns can be tracked from the forecast validation time back to at least day -6, with the sensitivity signal exhibiting downstream development characteristics in most cases. Bell et al. (2017) used ESA to investigate how extratropical cyclones relate to extreme wave events in the North Sea. They found that the largest extreme significant wave height events at an offshore platform in the central North Sea are associated with northerly-winds within extratropical cyclones which reach their maximum intensity. Weisman et al. (2015) applied ESA and identified that forecast area-averaged precipitation was sensitive to the southern extent of the upper trough over Colorado and to the lower-tropospheric meridional moisture transport over north-central Texas.

b. Motivation

Few studies have investigated sources of cyclone biases along the U.S. East Coast, including the cause of underdeepened or overdeepened cyclone intensity bias within the medium range operational numerical models. Lamberson et al. (2016) studied Joachim and found that synoptic scale errors originating in the warm sector of a cyclone can be a significant source of downstream forecast errors. Torn et al. (2015) focused on track position errors and found that hurricane Sandy's track position errors were related to the initialized water vapor mixing ratio, and to a lesser extent the upper-tropospheric horizontal divergence. Recent study of Lillo and Parsons (2016) extracted European forecast bust (large error) cases from 1990 to 2010 from ERA-Interim (data from ECMWF) forecasts. Their results implied that these busts happen in relation with the triggering and amplification of Rossby wave activity around the Atlantic, causing the large-scale pattern transitions. Zhu and Thorpe (2006) used an empirical way to compare the forecast error growth originating from the initial condition and the model uncertainties. They found that forecast error related to the initial uncertainties have 3 growth phases: an early initial phase of transient growth, an exponential

growth phase and saturation phase. For the experiments with model uncertainties, the forecast errors are initially 0 and increase with time to a power ranging from 0.5-3. After a certain amount of time, the model errors grow exponentially, followed by a saturation period. Korfe (2016) verified GEFS (Global Ensemble Forecast System) 20 ensemble members' track position mean average errors (Fig. 1a). As shown in figure 1a, the errors were interpolated to a 1.0° latitude-longitude grid and averaged over 8 cool seasons (Oct. 2007 ~ Mar. 2015) for medium range (72-144 h) forecast hours. Figure 1a shows the GEFS 20 ensemble members' cyclone errors density, which is cyclone error per cyclone number per square degree for large error cases in medium range (72-120 h). Using the GEFS CTL (control) member for hours 72-144 from the Korfe (2016) dataset, there is a cluster of overdeepened cyclone located in Nova Scotia region while large positive errors (underdeepened cyclones) are located more to the east of U.S. East Coast. Figure 1b shows that many of the large negative (overdeepened) errors occur farther north than large positive errors.

Figure 2 show the 2007-2015 cool season cyclones with larger mean sea level pressure error density distribution of GEFS 20 ensemble members. This is consistent with figure 1 that the negative errors are further to the north.

There has been no systematic analysis of the physical reasons for the underdeepened and overdeepened cyclone formation. Our research will address this by using cyclone relative field approach and analyzing different meteorological fields. There are still unaddressed questions related to this topic:

1. What physical ingredient for cyclogenesis may be leading to intensity biases?
2. What roles do moist dynamics play in terms of the cyclone intensity errors?

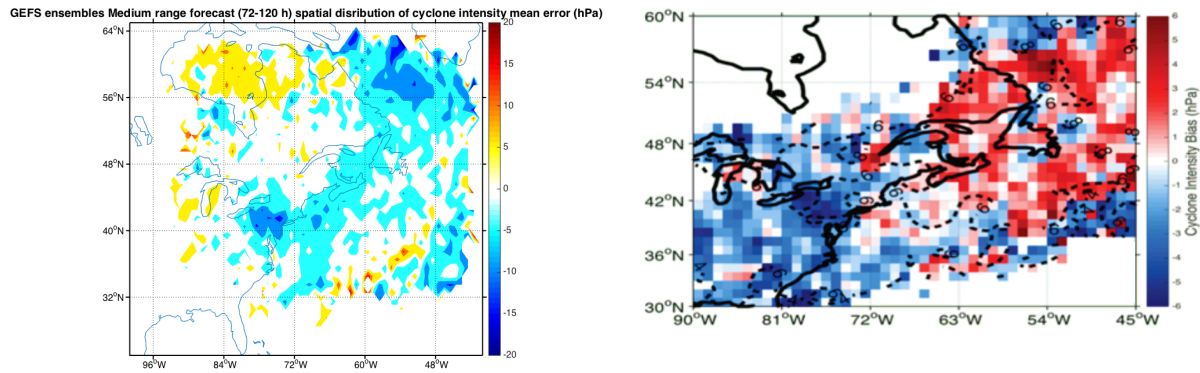


Fig 1. (left) 2007-2015 cyclone density errors (hPa: cyclone forecast errors per degree square per cyclone) plot

medium range forecast (72-120 h) spatial distribution in 20 GEFS ensemble members. (right) Medium range forecast (72-144 h) spatial distribution of cyclone intensity mean error (hPa) for NCEP GEFS ensemble

Dashed contoured values indicate the standard deviation (hPa) for each grid point. (Korfe 2016).

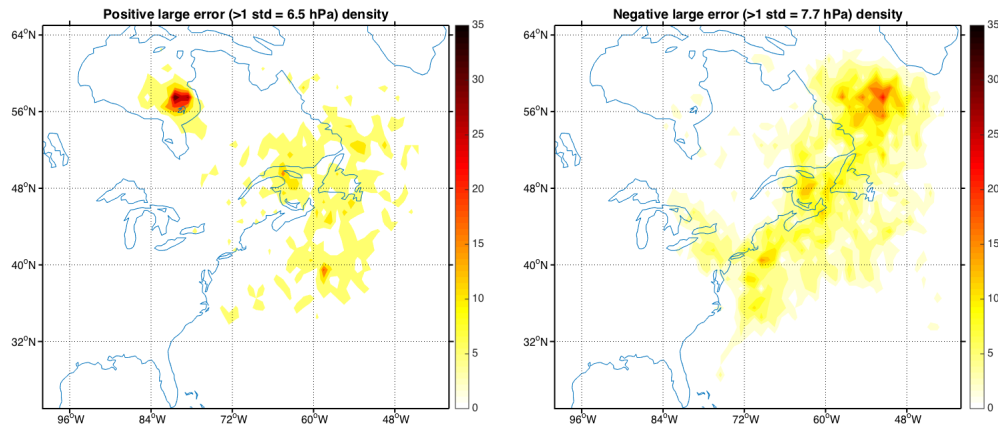


Figure 2. 2007-2015 cyclone density (cyclone numbers per degree square) plot for large (exceed one

standard deviation threshold) positive (left) and large neagative(right) error cases for underdeepening situation and overdeepening situation in 20 GEFS ensemble members for hour 102-120.

Chapter II: Data and Methods

a. Data

The Forecast data from GEFS control member and ensemble members forecast archived at TIGGE (THORPEX Interactive Grand Global Ensemble) were used. For the observed analysis data we use the ERA-interim analysis data from the TIGGE archive and for precipitation we used GPCP (Global Precipitation Climatology Project) global precipitation analysis daily data. The GEFS model current version is GFS V9.01 (Spectrum, Euler model). Its grid spacing is T254 (52-55km for 0-192 hours), T190 (70-74km for 192-384 hours), and vertical grid spacing is 42 hybrid levels with model top equals 2hPa. The GEFS data are 6 hourly. We utilized the mean sea level pressure, 500hPa geopotential height, integrated precipitable water, and potential temperature at 2PVU surface. The grid spacing for the data we use in GEFS forecast data is $0.5^\circ \times 0.5^\circ$ for most fields except precipitation and the corresponding ERA-interim resolutions are the same. The period of interest is the cool season (Oct to Mar) from Oct 2007 to Mar 2015 for the GEFS forecast data. The GPCP dataset is a merged analysis incorporating precipitation estimates from low-orbit-satellite microwave data, geosynchronous-orbit-satellite infrared data, and rain gauge observations (Huffman et al.

1997). The precipitation data grid spacing is $1^\circ \times 1^\circ$ and interval is 24 hours daily. Even if in this study the observational data is assumed to be correct, they have some limitations. In the Arctic, ERA-interim has positive biases in temperature and humidity below 850hPa compared to radiosondes (Dee et al. 2017). For the GPCP precipitation data, a relative error estimate for tropical land and ocean combined of 7% is obtained and an up to 50% increase of uncertainties are shown at higher latitudes (Adler et al. 2012).

b. Tracking and matching methods

The Hodges cyclone tracker was applied by Korfe (2016) using 6 hourly mean sea level pressure data for those cyclones within the area shown in Figure 3 (25N~65N; 100W~40W). A cyclone is tracked if it has a minimum lifetime of 24h and travels at least 1000 km within the domain. In order to match the cyclones in forecast and analysis data the pairing distance d of each point in an individual forecast track to each point in the analysis track must be less than the maximum pairing distance d_{\max} (1200 km). Second, at least 60% of the points in the forecast track had to coincide with the analysis track.

The Hodges approach tracks the anomaly pressure, not the total pressure. Colle et al. (2013) manually verified and hand tracked cyclones for 11 months (2286 cyclones) using the

same standard mentioned above and compared the results with the Hodges automated tracking scheme. They found that the probability of detection (POD) was 92.1% and the false alarm rate was 4.5%, so the uncertainty in the automated tracking results is likely between 5% - 15% for this study.

c. Cyclone relative approach

The initial testing of the cyclone relative approach focused on a box around the cyclone center that is 60 degree in the W-E direction and 40 degree in the N-S direction (Fig. 4). However, the size of cyclone relative box can be varied if needed. For ensembles cyclone relative plots, the box size is 250° longitude by 40° latitude. Several fields (mean sea level pressure, 500hPa geopotential height, integrated precipitable water, potential vorticity at 320K theta surface, etc.) were extracted and saved every 6 hourly from the forecast data and observation data in this boxed region. Difference error plots were created between the analysis and forecast cyclone.

d. “Box” method

The box method uses a small box to select data within it around the cyclone center and then average the data within this small box to calculate the distribution of these averaged

data. It was applied to temperature gradient at 925 hPa and precipitation field. It helps to address what error type individual cases would have.

e. Case selection.

We selected a few hundred cases to test the cyclone relative approach based on the central pressure error exceeding a certain threshold for the day 4-5 forecast. First, the average MSLP error is obtained for all cyclone centers during hours 102 - 120. If the average of cyclone errors exceeds a specific pressure threshold, the cyclone is considered to be a large error case. The large error could be either negative (overdeepening) or positive (underdeepening) given the sign of the error. If the same cyclone can be tracked back to hour 54, it is considered Lagrangian error cases. If we don't require the cyclone to be tracked back to particular time, these are considered instantaneous error events. For the GEFS verification, we had two types of error cases. One is if the average exceeds one standard deviation (8.2hPa, -8.0hPa; Fig. 6) for the instantaneous cases, while if the average error exceeds a half standard deviation (+4.2hPa, -3.9hPa) for the Langrangian error events.

f. Ensemble sensitivity analysis (ESA) method.

The sources of variability contributing to the errors can also be diagnosed through an

ensemble sensitivity analysis. As used by Chang et al. (2013) and Zheng et al. (2013), ESA is

given by:

$$ESA = \frac{\text{COV}(x,p)}{s_x s_p} \quad (1)$$

where x is a gridded variable and p is the response function. In this case, p is chosen to be the

projection coefficient of ensemble members anomaly projecting on ensemble mean error of

mean sea level pressure. S_x and S_p are the sample standard deviations of x and p respectively.

The orthogonal projection of $y \in C^N$ onto $x \in C^N$ is defined by:

$$Px(y) = \frac{\langle y, x \rangle}{\|x\|^2} x \quad (2)$$

The scalar $\frac{\langle y, x \rangle}{\|x\|^2}$ is called the coefficient of projection. From figure 7, when y is projected

onto a unit length vector x , the coefficient of projection is simply the inner product of y with

x .

We will use the projection coefficient of each ensemble member's anomaly projected on

ensemble mean error.

$$\text{ANO} = \text{each member's sea level pressure anomaly} \quad (3)$$

$$\text{EME} = \text{ensemble mean sea level pressure error} \quad (4)$$

$$\text{Proj(ANO-} \rightarrow \text{EME)} = (\text{ANO.EME}) / (\text{EME.EME}) \quad (5)$$

In fact, one can easily show that if one defines

$$\text{MEME} = \text{each member's sea level pressure error} \quad (6)$$

$$\text{Proj}(\text{MEME} \rightarrow \text{EME}) = (\text{EME} + \text{ANO}) \cdot \text{EME} / (\text{EME} \cdot \text{EME}) = 1 + \text{Proj}(\text{ANO} \rightarrow \text{EME}) \quad (7)$$

The second index shows the error spread of ensemble members.

For how we correlate and get the ESA, like shown in figure 8, first, calculate the projection coefficient within the small box around the cyclone and correlate hour 120's projection coefficient with the larger cyclone relative domain. The size of the cyclone relative domain could vary but for later examples they are 240 degrees longitude x 40 degrees latitude. The area for calculating the projection coefficient is 30 degrees longitude x 30 degrees latitude.

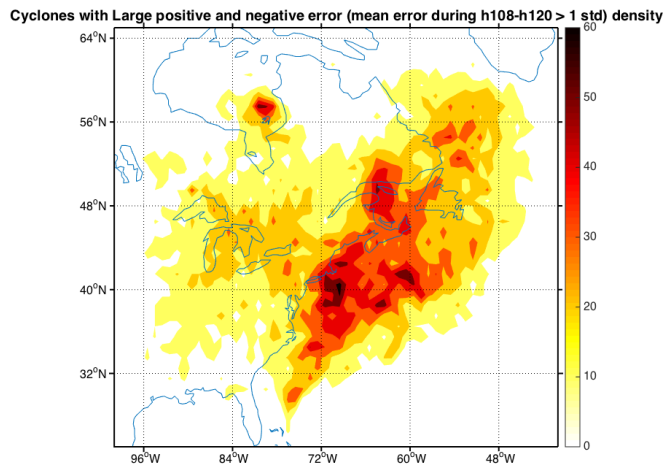


Figure 3. Locations where cyclones are tracked and the 2007-2015 cyclone density (cyclone numbers per degree square) distribution of all time step tracks of cyclones which have large positive and negative errors during hour 108 - 120 in 20 GEFS ensemble members.

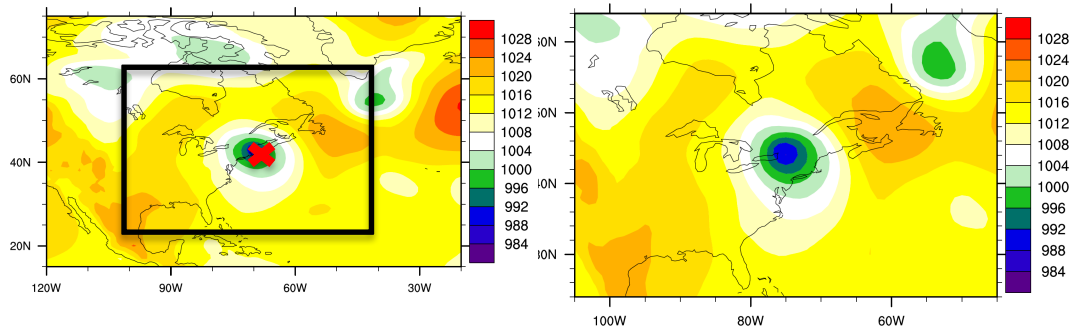


Figure 4. (Left) the mean sea level pressure (hPa, shaded), the black box shows the cyclone relative domain and red x shows the cyclone center. (Right) the extracted cyclone relative field.

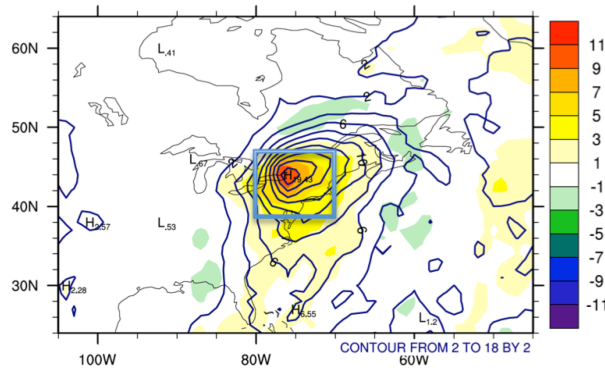


Figure 5. Example of box method area.

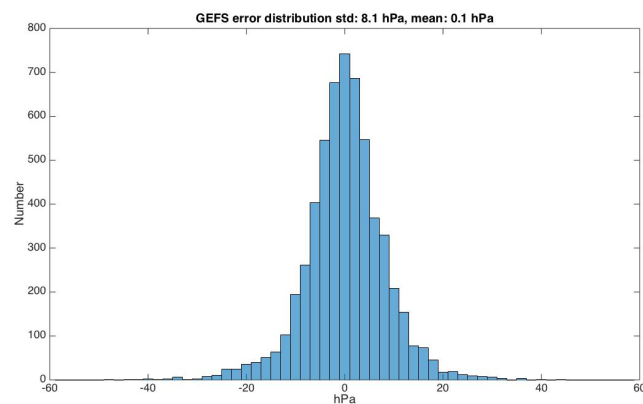


Figure 6. GEFS error distribution. The mean is 0.1hPa, and standard deviation is 8.1hPa. All cyclone cases of GEFS control member and all time steps are included.

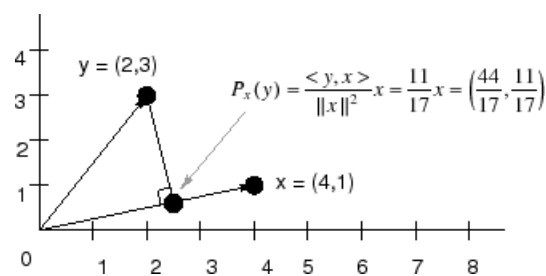


Figure 7. projection of y on x in 2D space. Cite from <https://www.dsprelated.com/freebooks/mdft/Projection.html>

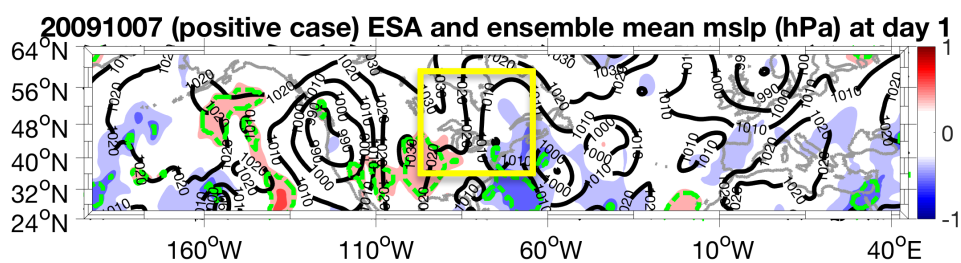


Figure 8. Yellow small box area is projection coefficient calculation area. Larger domain is ESA calculation area.

Chapter III: Cyclone relative approach results

a. Mean sea level pressure results

Figure 9 shows the mean sea level pressure from hour 54 to hour 120 with plotting domain 40° latitude x 60° longitude in GEFS control member. For the overdeepened cases, the averaged model central low varies from 994 hPa at day 3 to 990 hPa at day 4 and then 986 hPa at day 5. For the underdeepened cases, the averaged model central low varies from 1001 hPa at day 3 to 1000 hPa at day 4 and then 998 hPa at day 5. The mean sea level storm looks similar to relative plots in Northwest Atlantic shown by Wang and Rogers (2001) since both are nearly circular in shape. The mean sea level pressure cyclone center errors are relatively small (< 1 hPa) at hour 54 to 72 (day 3), then grow rapidly at hour 78 to hour 120 (day 5) to around 12 hPa. The small errors can spread around the map, but most the errors are located at the center of the cyclones. Mean sea level pressure errors in overdeepened and underdeepened cases are statistically significant for all 3 days.

Figure 10 shows the GEFS control member mean sea level pressure overdeepened cases error minus underdeepened cases error differences. It indicates there is a negative 20 hPa

differences between overdeepened and underdeepened cases error at day5. The error

difference is statistically significant for all 3 days.

b. PV (potential vorticity) at 320K theta level results

In figure 11, the PV model maximum has a trough like structure in the west side of cyclone center in all time steps. For both the overdeepened and underdeepened cases, PV value in the north side of cyclone center is lower (0.6 PVU for overdeepened cases and 0.8 PVU for underdeepened cases) in the model. The PV value at west side of cyclone center is higher in the overdeepened cases (around 0.8 PVU larger) and lower in the underdeepened cases (around 1.4 PVU less) at day 5. The negative errors in underpredicted cases seem transport from the north through day 3 to day 5 while the positive errors in overpredicted cases grow locally. This make sense because that the overdeepened cyclones should have stronger PV while the underdeepened cyclones have weaker PV. PV errors at 320K for the overdeepened and underdeepened cases are statistically significant for all 3 days over whole map.

Figure 12 shows the GEFS control member PV at 320K overdeepened cases error minus underdeepened cases error differences. It implies there are positive 2 PVU differences

between overdeepened and underdeepened cases error at day 5. The error difference is statistically significant for all 3 days.

c. 925 hPa temperature gradient results

In figure 13, outside of the cyclone center the 925 hPa temperature gradient cyclone relative error is negative, which means the model temperature gradient is weaker in most areas. The maximum temperature gradient for the overdeepened cases decrease from 33.28 K/ 10^3 km to 31.02 K/ 10^3 km from day 3 to day 5. For the underdeepened cases, the maximum temperature gradient increases from 25.75 K/ 10^3 km to 29.95 K/ 10^3 km from day 3 to day 5. For the overdeepened cases there is little errors in the temperature gradient around the cyclone at day 3, but by day 5 the model has stronger temperature gradient along the cold front. For the underdeepened cases the model has weaker gradient closer to the cyclone center and along the cold front for days 3-5. The 925 hPa temperature gradient errors in both overdeepened and underdeepened cases are statistically significant for all 3 days.

Figure 14 shows the GEFS control member 925 hPa temperature gradient overdeepened cases error minus underdeepened cases error differences. It indicates there are positive 10

$\text{K}/10^3\text{km}$ differences between overdeepened and underdeepened cases error at day 5 at the cold front area. The error difference is statistically significant for all 3 days.

Figure 15 of the box area daily average errors distributions show that positive temperature gradient errors at 925 hPa dominate for overdeepened cases on day 4 and day 5 and negative temperature gradient errors dominate for underdeepened cases for all 3 days. For overdeepened cases, only the day 5 mean is significantly different from 0 while for underdeepened cases, all the 3 days means are significantly different from 0. At day 3, overdeepened and underdeepened distribution are significantly different.

d. Precipitation results

From figure 16, the model contours of precipitation have comma shaped structures on the east of cyclone centers. For overdeepened cyclones, the center highest precipitation decreased from 22.3 mm/day to 19.4 mm/day from day 3 to day 5, and for underdeepened cyclones, the center maximum precipitation decreased from 17.9 mm/day to 16.5 mm/day form day 3 to day 5. It can be seen that the model has more precipitation than observation and the error is positive in most areas. The overdeepened cases have more positive errors on the southern part of cyclone center (larger around 10 mm/day in day 4). The results are consistent with

previous studies (Field et al. 2008, Hawcroft et al. 2015), which found that the global models tend to overestimate the precipitation around a cyclone. To the north of underdeepened cases, there are negative errors (less than 6 mm/day in day 4), which means that the latent heat release is greater in overdeepened cases than in underdeepened cases. The precipitation pattern is significant on day 3, while the cyclone center pressure error in day 3 is small (Fig. 9), moisture and hence latent heat released by it may contribute to cyclogenesis intensity errors. Precipitation errors in overdeepened and underdeepened cases are not statistically significant for all 3 days.

Figure 17 shows the GEFS control member precipitation overdeepened cases error minus underdeepened cases error differences. It indicates there are positive 15 mm/day differences between overdeepened and underdeepened cases error at day 3 and day 4. The error difference is statistically significant for all 3 days.

Figure 18 of the box area daily average errors distributions show that positive precipitation errors dominate for overdeepened cases and the mean error is negative but not statistically significant for only day 3 and 4 for underdeepened cases. For overdeepened cases, all 3 days means are significantly different from 0 while for underdeepened cases, all 3

days means are not significantly different from 0. At day 3, overdeepened and underdeepened distribution are significantly different. Overall, this suggests with the positive precipitation errors for the overdeepened cases that excessive latent heating may be contributing to the overdeepening errors.

The correlation between 925 hPa temperature gradient and precipitation at day 3 for overdeepened cases are -0.28 and significant. While for other days both overdeepened and underdeepened cases are with relatively low correlation and not significant.

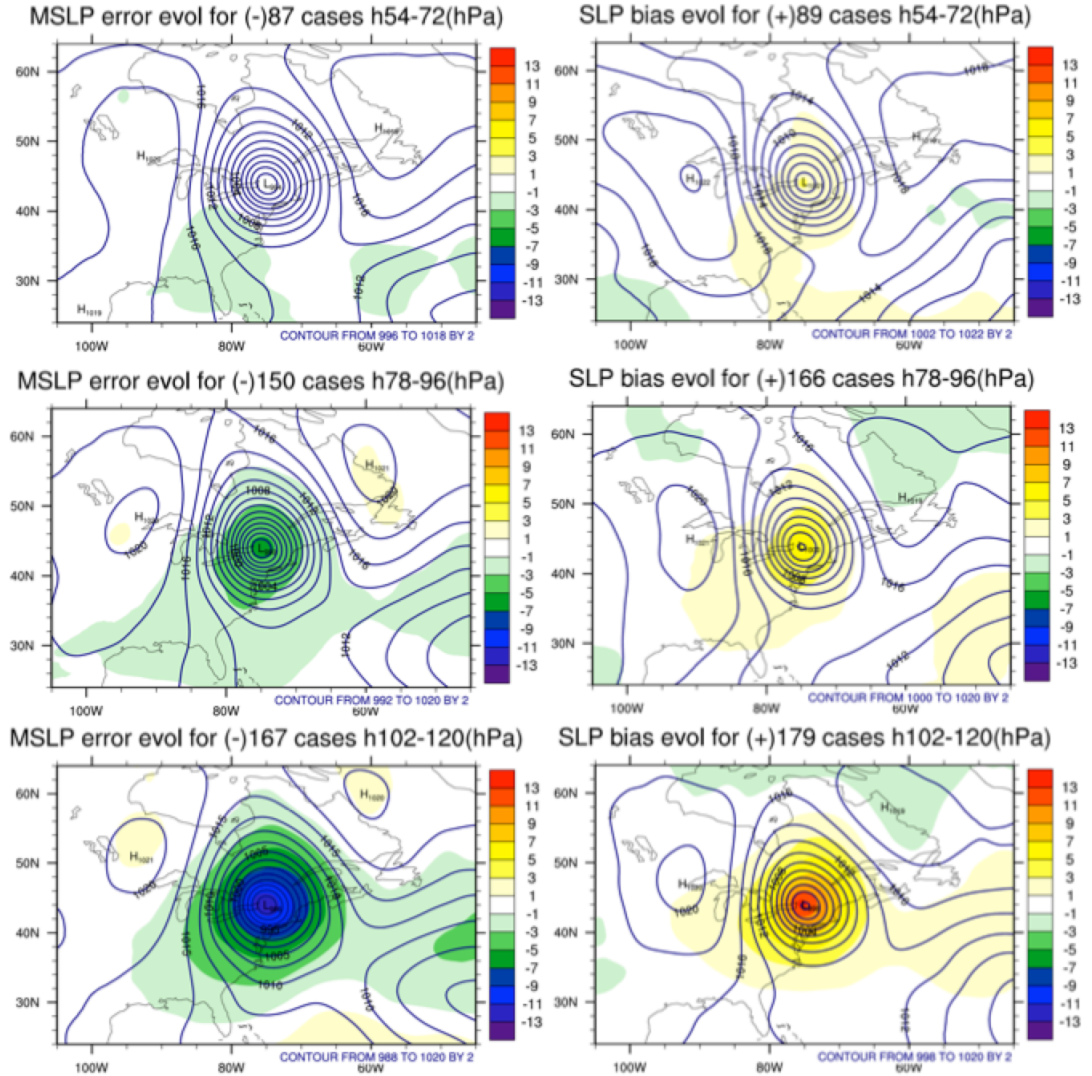


Figure 9. GEFS control member mean sea level pressure relative error (shaded; model minus analysis) and model forecast (contoured) for overdeepened cases (left) and underdeepened cases (right) at hour 54-72 (top), 78-96 (middle) and 102-120 (bottom).

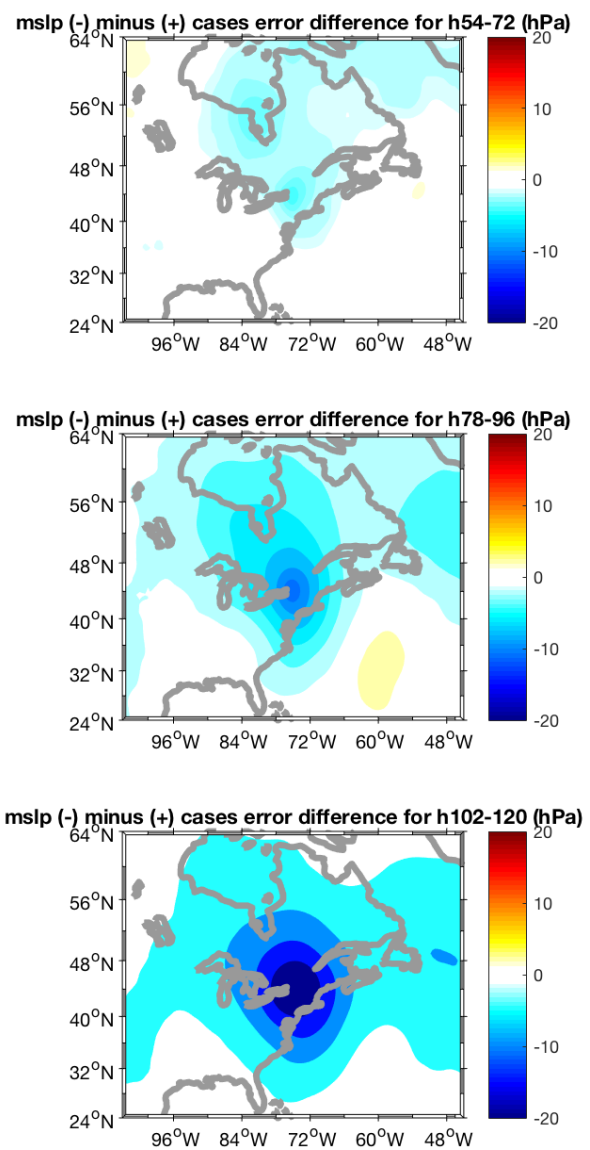


Figure 10. GEFS control member mean sea level pressure (hPa) overdeepened cases error minus underdeepened cases error at hour 54-72 (top), 78-96 (middle) and 102-120 (bottom).

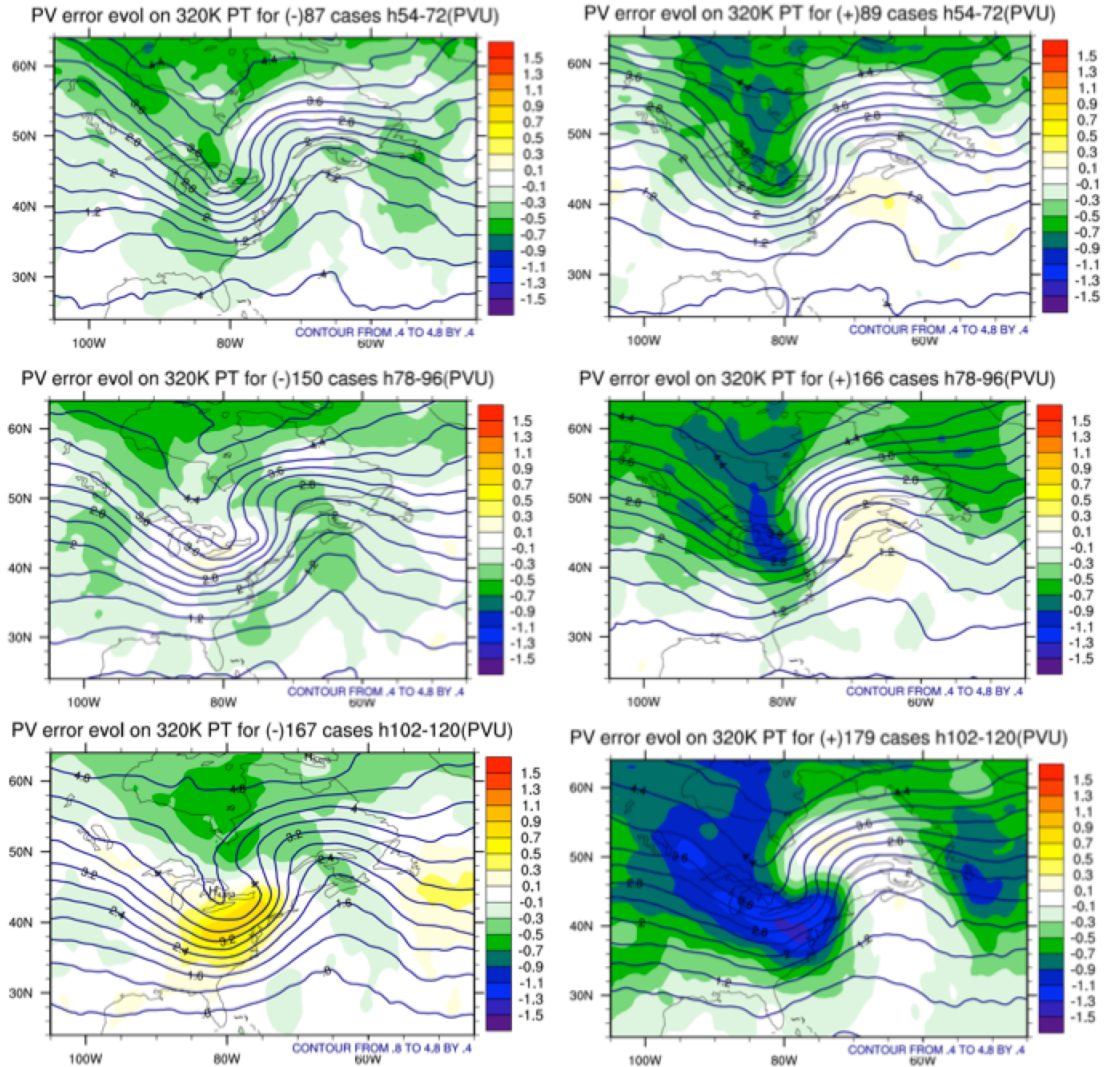


Figure 11. GEFS control member PV (potential vorticity) at 320K theta level relative error (shaded; model

minus analysis) and model forecast (contoured) for overdeepened cases (left) and underdeepened cases (right) at hour 54-72 (top), 78-96 (middle) and 102-120 (bottom).

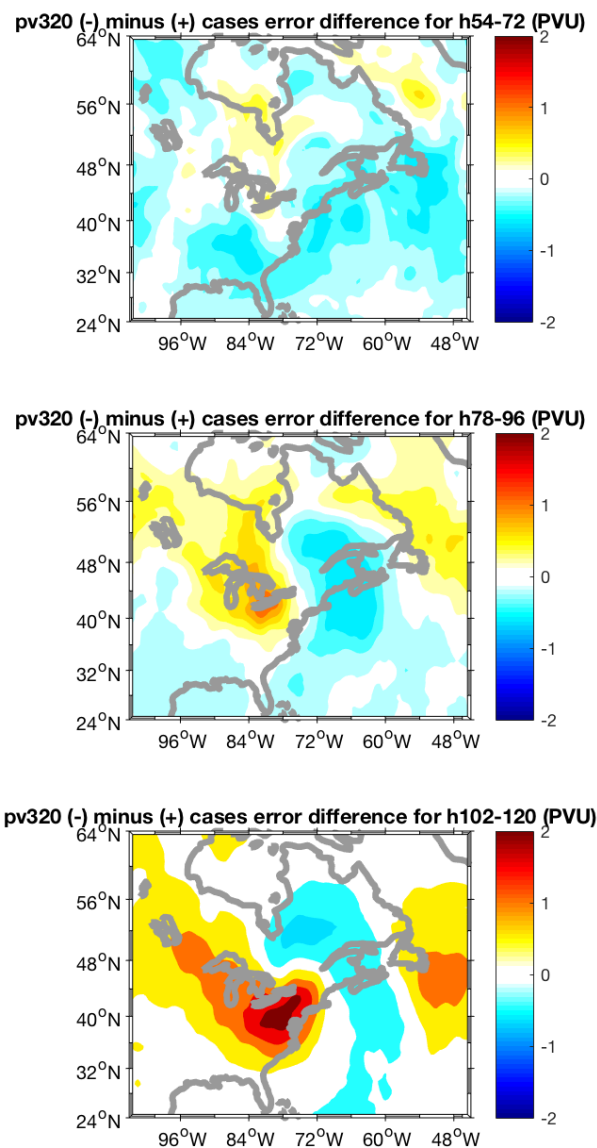


Figure 12. GEFS control member potential vorticity at 320K (PVU) overdeepened cases error minus underdeepened cases error at hour 54-72 (top), 78-96 (middle) and 102-120 (bottom).

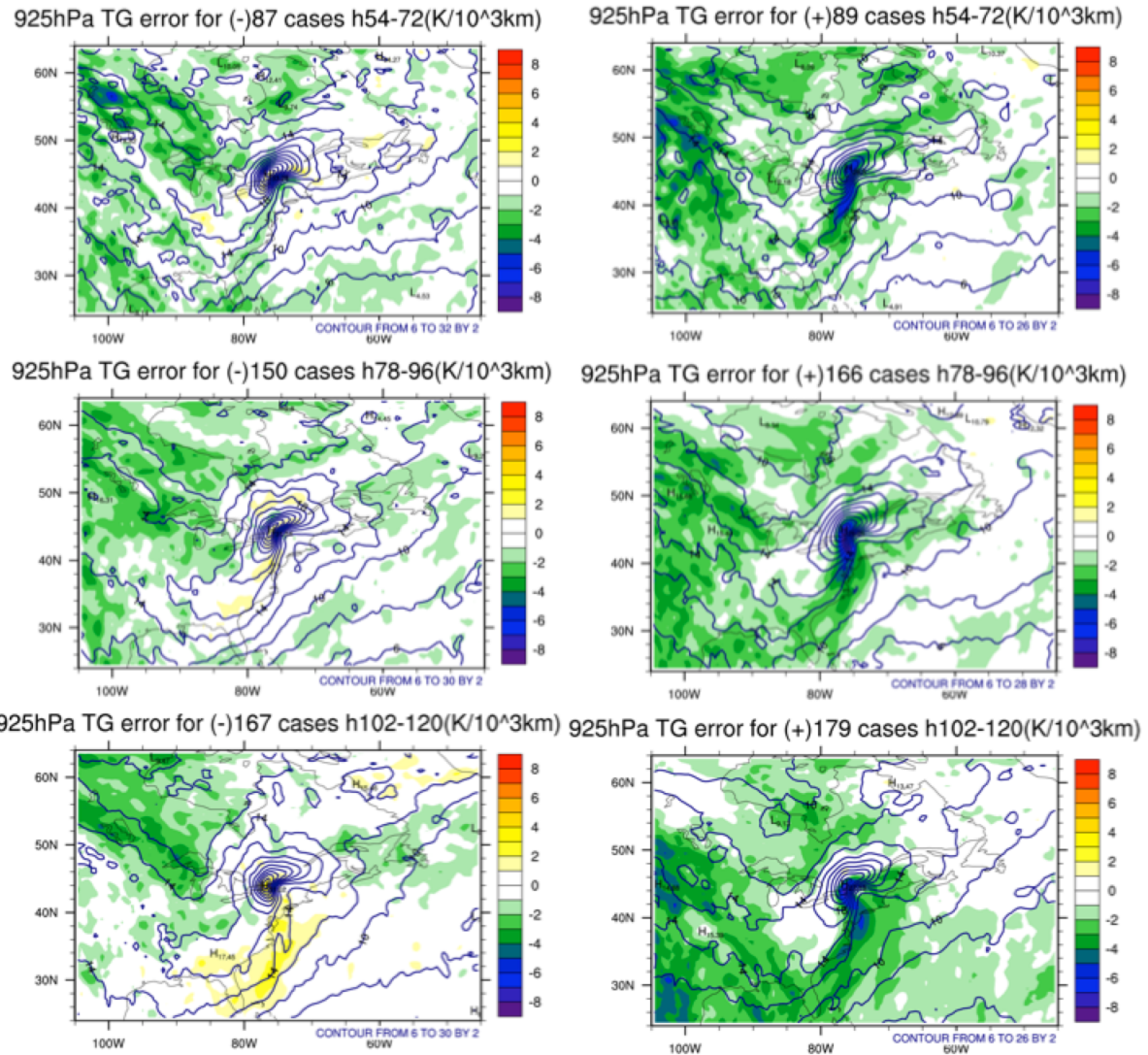


Figure 13. GEFS control member 925 hPa temperature gradient relative error (shaded; model minus analysis)

and model forecast (contoured) for overdeepened cases (left) and underdeepened cases (right) at hour 54-72 (top), 78-96 (middle) and 102-120 (bottom).

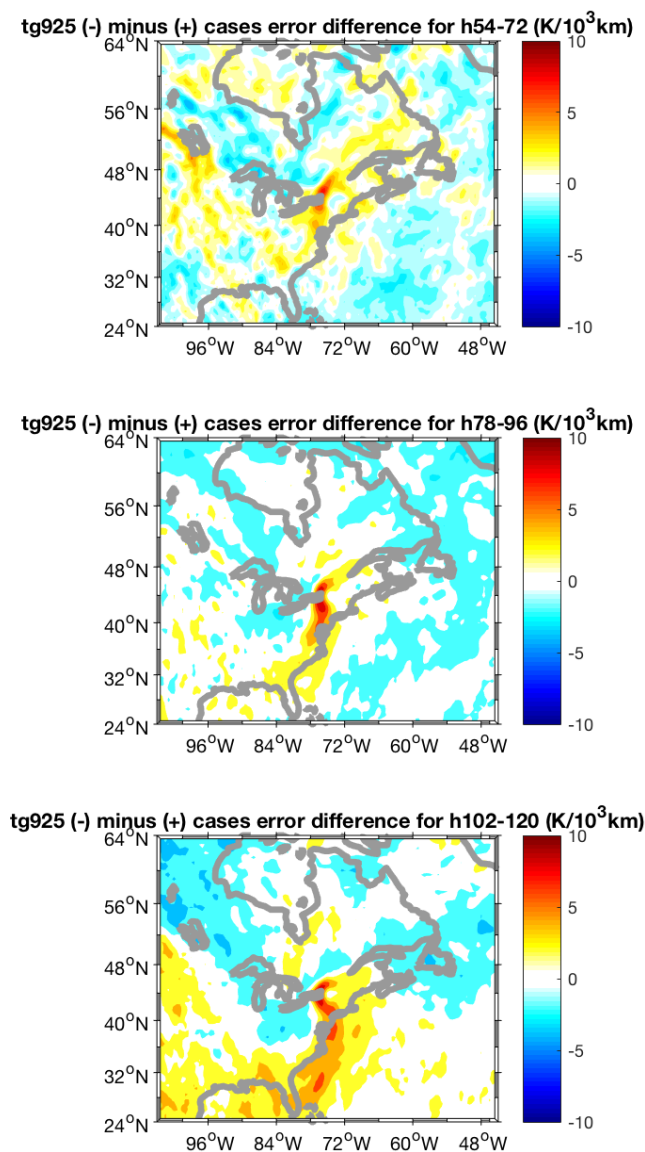


Figure 14. GEFS control member temperature gradient at 925 hPa (K/10³km) overdeepened cases error minus underdeepened cases error at hour 54-72 (top), 78-96 (middle) and 102-120 (bottom).

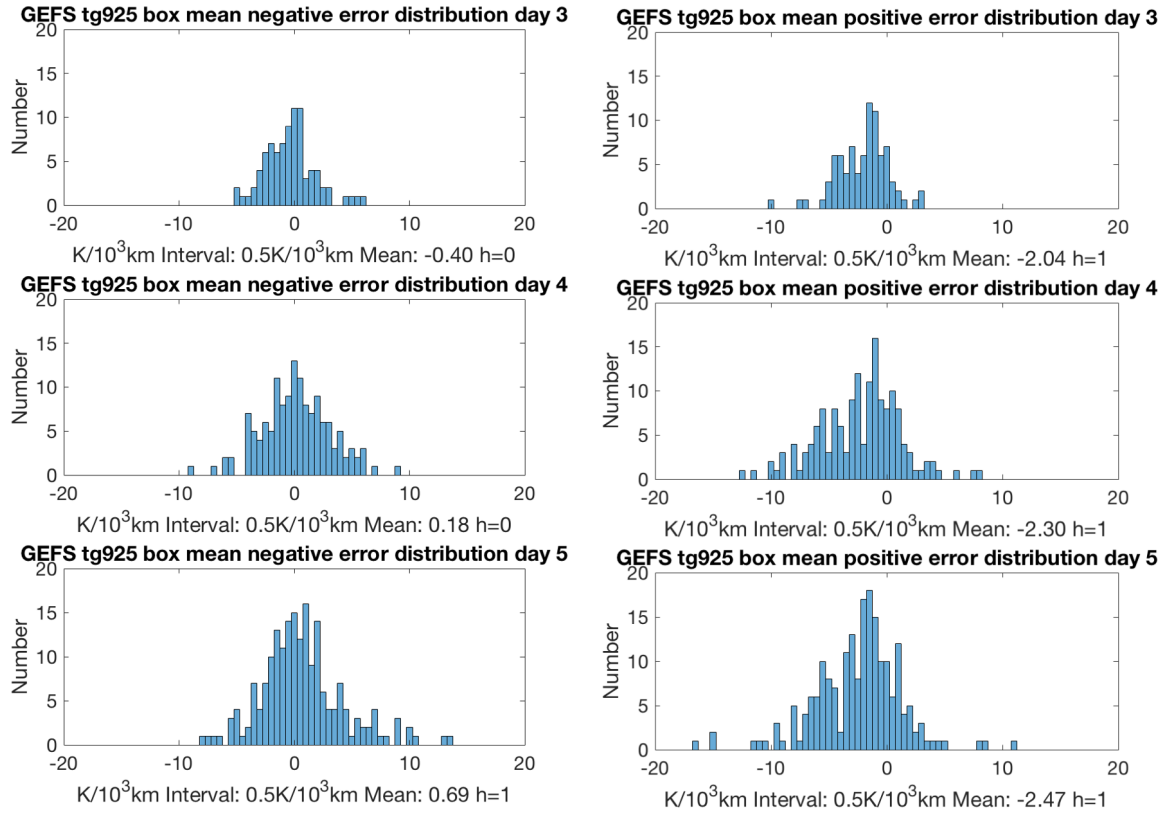


Figure 15. GEFS control member 925 hPa temperature gradient box area (shown previously) daily averaged

errors for overdeepend cases (left) and underdeepend cases (right) distributions at day 3 (top), day 4 (middle) and day 5 (bottom). $h=1$ means the mean of this distribution is significantly different from 0 and $h=0$ means the opposite.

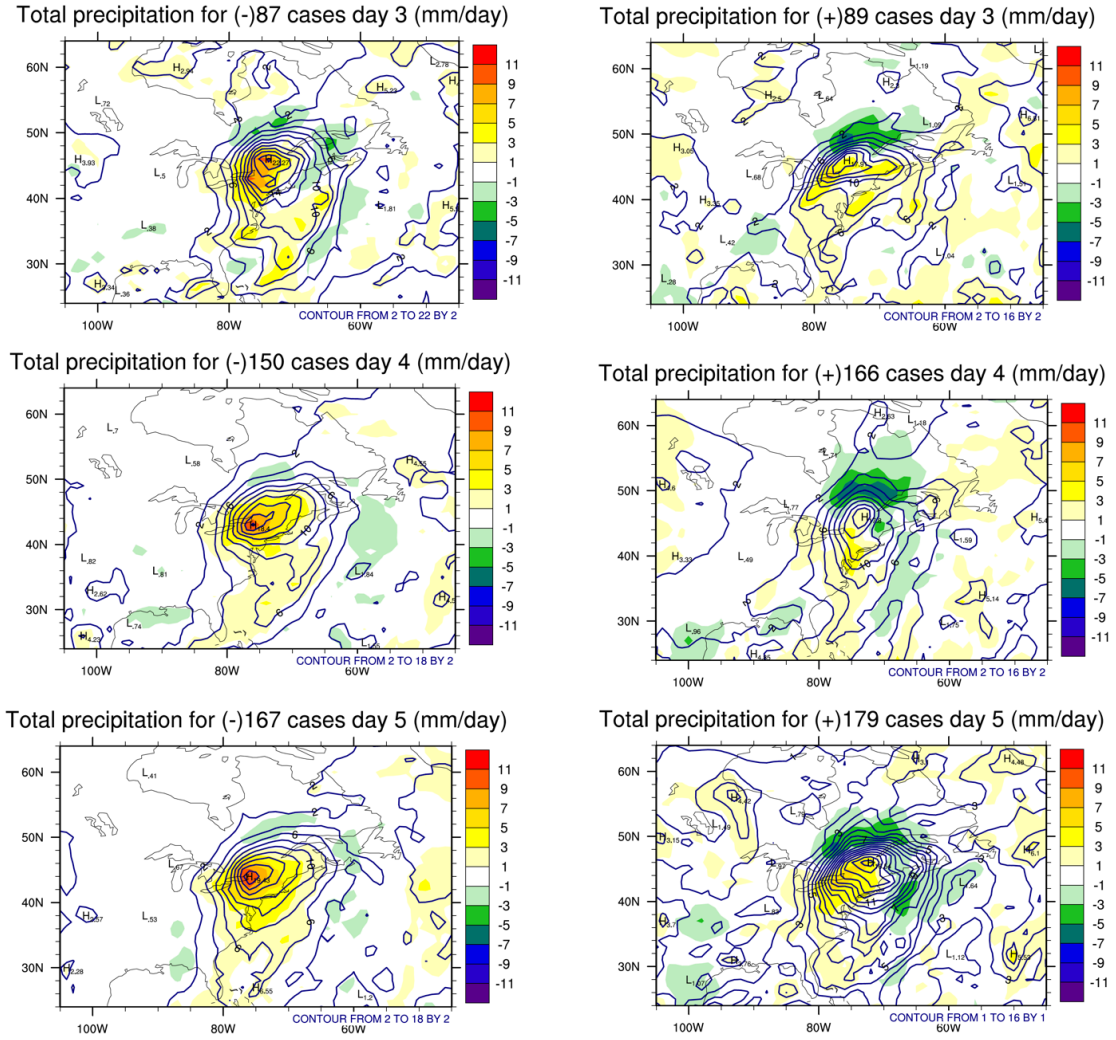


Figure 16. GEFS control member precipitation relative error (shaded; model minus analysis) and model forecast (contoured) for overdeepened cases (left) and underdeepened cases (right) at day 3 (top), day 4 (middle) and day 5 (bottom).

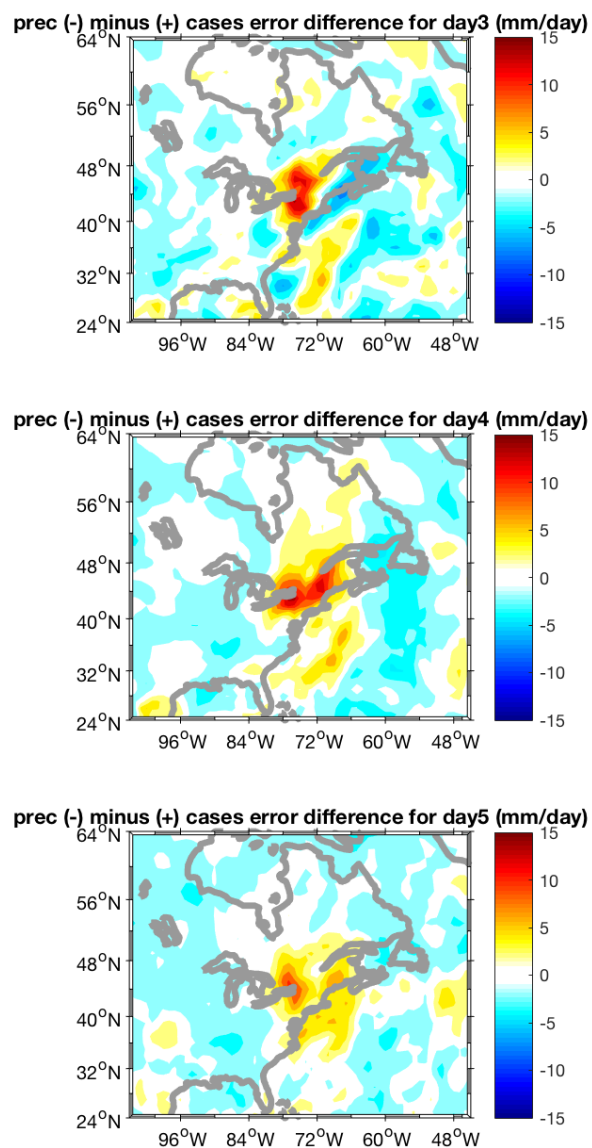


Figure 17. GEFS control member precipitation (mm/day) overdeepened cases error minus underdeepened cases error at day3 (top), day4 (middle) and day5 (bottom).

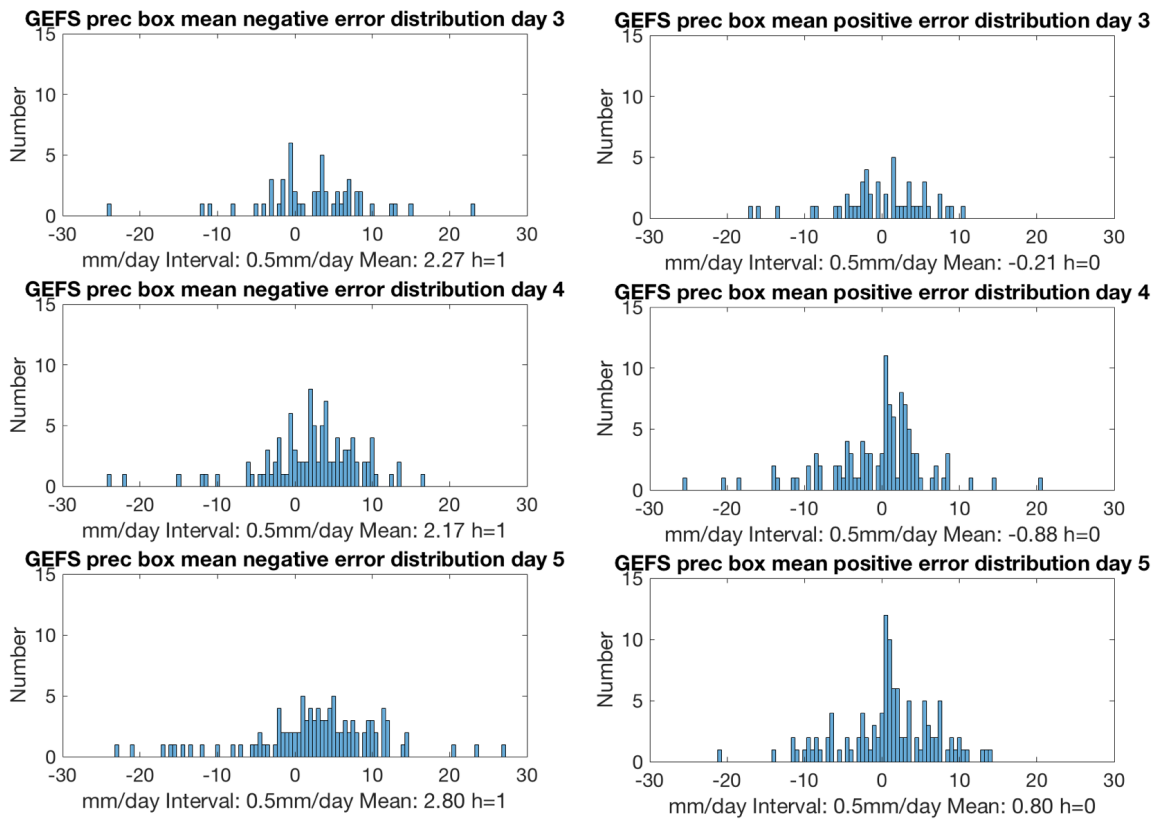


Figure 18. GEFS control member precipitation box area (shown previously) daily averaged errors for overdeepend cases (left) and underdeepend cases (right) distributions at day 3 (top), day 4 (middle) and day 5 (bottom). h=1 means the mean of this distribution is significantly different from 0 and h=0 means the opposite.

Chapter IV: Ensemble sensitivity single case studies

a. 30 January 2010 overpredicted case

Figure 19 shows the ensemble sensitivity and ensemble mean of mean sea level pressure starting on 30 January 2010 for an overpredicted case from the GEFS model. 30 January 2010 is day 1. It is 20 ensemble members' mean and is cyclone relative domains with 240° in longitude and 40° in latitude. The reason that only these 3 cases are shown is that they have relatively better results in ESA correlations. The 3 other cases tested which has poor ESA correlation especially of total column water are 19 March 208, 26 October 2012 and 16 March 2015. The ensemble mean contours suggest that at day 1, the cyclone center is not clear with a center minimum pressure of 1005 hPa. The cyclone center deepens from 990 hPa on day 2 and deepens to below 970 hPa on day 3, below 960 hPa on day 4, and then becomes less deep on day 5 (980 hPa). The ensemble sensitivity analysis (ESA) on day 1 shows incoherent patterns that disappear by day 2. By days 2 and day 3, the correlation has a certain pattern which is positive correlation to the north and negative correlation to the south, but it's not that statistically significant. On day 4, the pattern becomes more defined, with a positive correlation on the northwest of cyclone center and negative correlation on the south of

cyclone center. This suggests that if the ensemble mean sea level pressure is higher in on the cyclone's northwest side, then the error projection coefficient will be larger, or each member's error projection on ensemble mean error will be larger. The signal partially reflects that the cyclone intensity error will be larger if the northwest side ensemble mean sea level pressure will be higher. It should also be noted that there's positive correlation coming from an upstreams location. For the south part of cyclone center, if the mean sea level pressure of the ensemble mean will be lower, then the error projection coefficient will be larger. The signal implies that if the cyclone center is forecast to be more northwestward, the error will be smaller.

Figure 20 displays the geopotential height results at 700 hPa for the overprediction case. At days 1 and 2, the ensemble mean height shows a trough structure positioned over the developing cyclone. From day 3, a low is formed and the center height stays around 2600 m. In terms of the ensemble sensitivity correlation, it is not significant on day 1 and day 2. From days 3 to day 5, the ESA has similar pattern as that of mean sea level pressure. There is a positive correlation on the north side of cyclone center and a negative correlation just in the

center of cyclones. There is also an upstream positive correlation. It is suggested that the errors will be smaller if the 700 hPa low moves northeast ward.

Figure 21 shows the results for total column water. A ridge like structure of ensemble mean total column water is around south side of cyclone center. This implies that the warm conveyor belt transport moisture to northeastward (Eckhardt et al. 2004). The ensemble sensitivity correlation is not significant until day 3. There is a positive correlation around the cyclone center. This means that the cyclone pressure errors will be smaller if the total column water decreases. Thus, an overpredicted cases has too much more moisture in the modeling system.

In this case, the large and significant correlation happens later and mostly in day 4 and day 5 for most fields. The ESA of mean sea level pressure and geopotential at 700hPa are negative in cyclone center area, implying that the error will increase as the contours decrease (the system gets deeper). The total column water center correlation is positive, meaning that the error will increase if total column water increases, leading to an overprediction of total column water.

b. 7 October 2009 underpredicted case

Figure 22 shows the ensemble sensitivity and ensemble mean of mean sea level pressure starting on 7 October 2009 for an underpredicted case. 7 October 2009 is day 1. The ensemble mean sea level pressure of the cyclone center pressure decreases from 1010 hPa to 1000 hPa between days 1 and 5, respectively. The ensemble sensitivity shows positive correlation to the west side of the cyclone and negative correlation to the east of cyclone center on days 1 and 5, while other days the positive correlation to the west dominates. It implies that on west side of the cyclone center, the error projection coefficient would be larger if the ensemble mean mean sea level pressure gets higher, and the opposite applies on east side of cyclone center. This means if the cyclone move westward, the error projection coefficient would be smaller. The ensemble sensitivity also shows an upstream influence of positive correlation.

Figure 23 shows the bad member minus good member's difference and ensemble mean results. These results help confirm whether the ESA correlation regions are reliable. There are 11 bad members and 5 good members, with the bad members' cyclone center pressure exceeding 10 hPa and good members' cyclone center pressure are less than 6 hPa. On day 4

and day 5, the bad minus good members' results are very similar to that of ESA correlation.

This indicates that the ESA results are reliable.

Figure 24 shows geopotential height results at 700 hPa for the underpredicted case.

There's a low aloft since day 1. The minimum geopotential height keeps around 2850 gpm.

For the ensemble sensitivity correlations, the positive correlation prevails on northwest of

cyclone center, which is similar to that of mean sea level pressure correlations.

Figure 25 shows the bad minus good members results for geopotential height at 700 hPa.

It also has very similar difference pattern as the ESA correlation pattern that is positive

correlation to the west and negative correlation to the east.

Figure 26 displays the results for total column water for the underpredicted case.

Regarding the total column water contours, there is a cyclone on the west side of the cyclone

that is underpredicted, and two ridge-like structures are apparent. The western ridge extends

to the north and the central one stays more locally. As for the ensemble sensitivity

correlation, it first shows up locally at day 1 negatively with high significance. Then the area

that should be considered as warm conveyor belt of the western cyclone gradually generates

the negative correlation, indicating that if the total column water increases, the cyclone

intensity error projection coefficient would be smaller. It implies that moisture is responsible for cyclogenesis intensity errors.

Figure 27 shows the bad minus good members results total column water. The large negative difference happens on the warm conveyor belt area of the western cyclone. This pattern matches with the ESA correlation pattern.

If the system gets weaker and the total column water decreases, the anomaly to mean error projection coefficient would get larger. Sea level pressure and 700hPa height ESA plots suggest the upstream features are too weak. There seems to be some suggestion of underprediction of upstream moisture with this underpredicted case, so there may be a diabatic heating contribution that was underforecast in the ensemble.

c. 12 October 2011 underpredicted case

Figure 28 presents the ensemble sensitivity and ensemble mean of mean sea level pressure starting on 12 October 2011 for an underpredicted case. 12 October 2011 is day 1. The ensemble mean contours of mean sea level pressure doesn't have a closed cyclone until day 3 with minimum intensity stays around 985-990 hPa. The positive ensemble sensitivity correlation governs the pattern during the whole forecast days while large significant negative

correlation appears around other cyclones in plots on day 5. This pattern implies that if the cyclone moves northward a little bit, the error projection coefficient would be smaller.

Figure 29 shows geopotential height results at 700 hPa for the underpredicted case. For the ensemble mean contours of geopotential height at 700 hPa, there is a cyclone on days 4 and 5, with center minimum geopotential height of about 2750-2800 m. Similar to the pattern found in mean sea level pressure, the positive correlation dominates during whole forecast days while negative correlation show up in day 5.

Figure 30 presents the total column water for the underpredicted case. For the ensemble mean contours, the ridge-like structures are located at cyclone centers in the plots at beginning, while the number decreases to one that belongs to the underpredicted cyclone of focus on day 5. The ensemble sensitivity correlation is initially noisy, but by days 4 and 5 it forms a pattern that positive correlation to the northwest and negative correlation to the northeast of cyclone centers. It indicates that if the total column water decreases on the west side of cyclone center, the error projection coefficient decreases and the opposite applies to the east of cyclone center.

The center correlation is mainly positive for mean sea level pressure and geopotential

height at 700hPa, so the error will increase if the contours increase (the system gets weaker).

For total column water, there is negative correlation to the east and positive correlation to the west. This suggests that the warm conveyer belt region on the east is underpredicted in total column, which makes the system weaker.

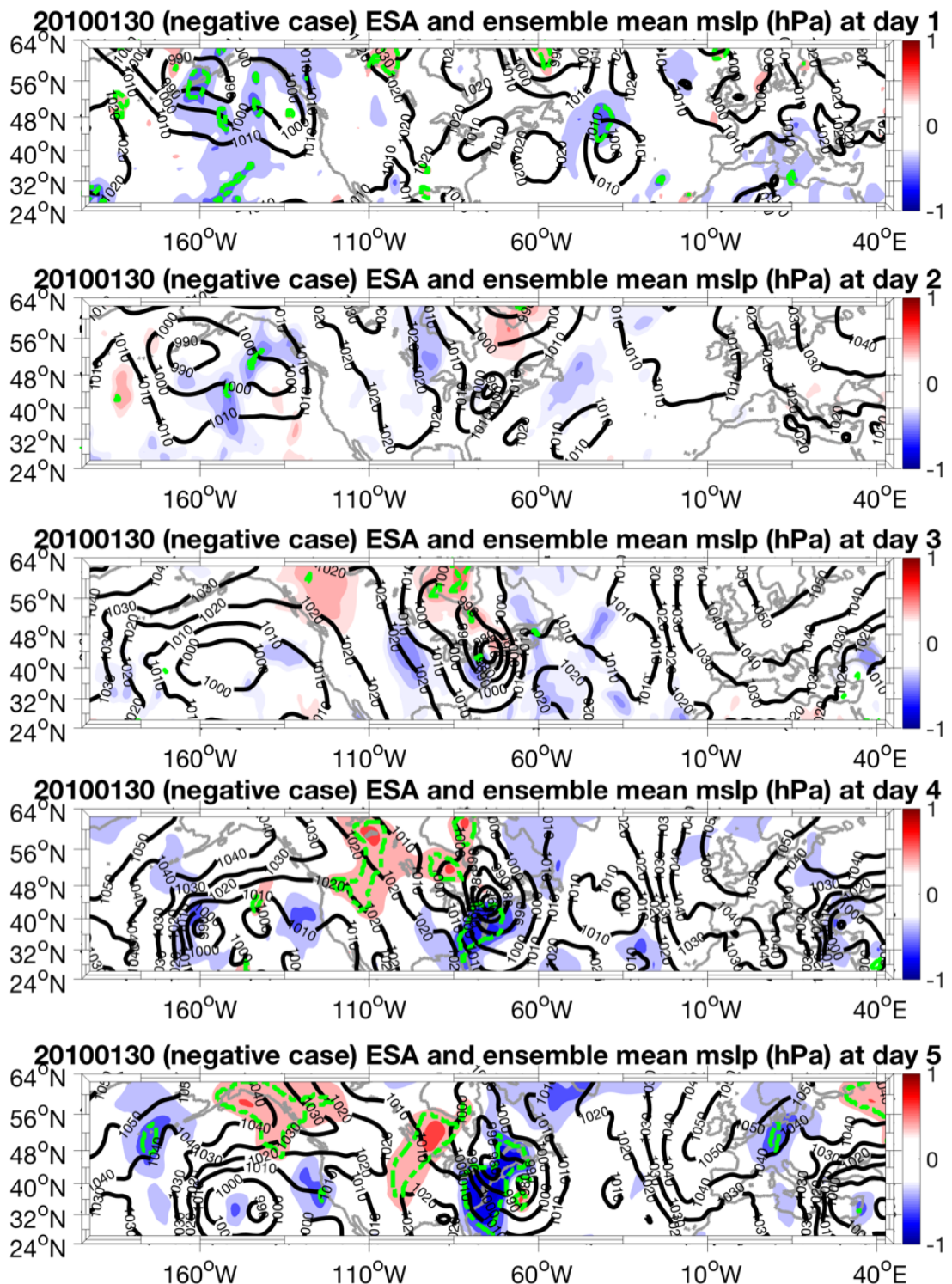


Figure 19. 20100130 (overpredicted case) daily ensemble sensitivity (shades) and ensemble mean mean sea level pressure (contours). The green line area has significance over 95%.

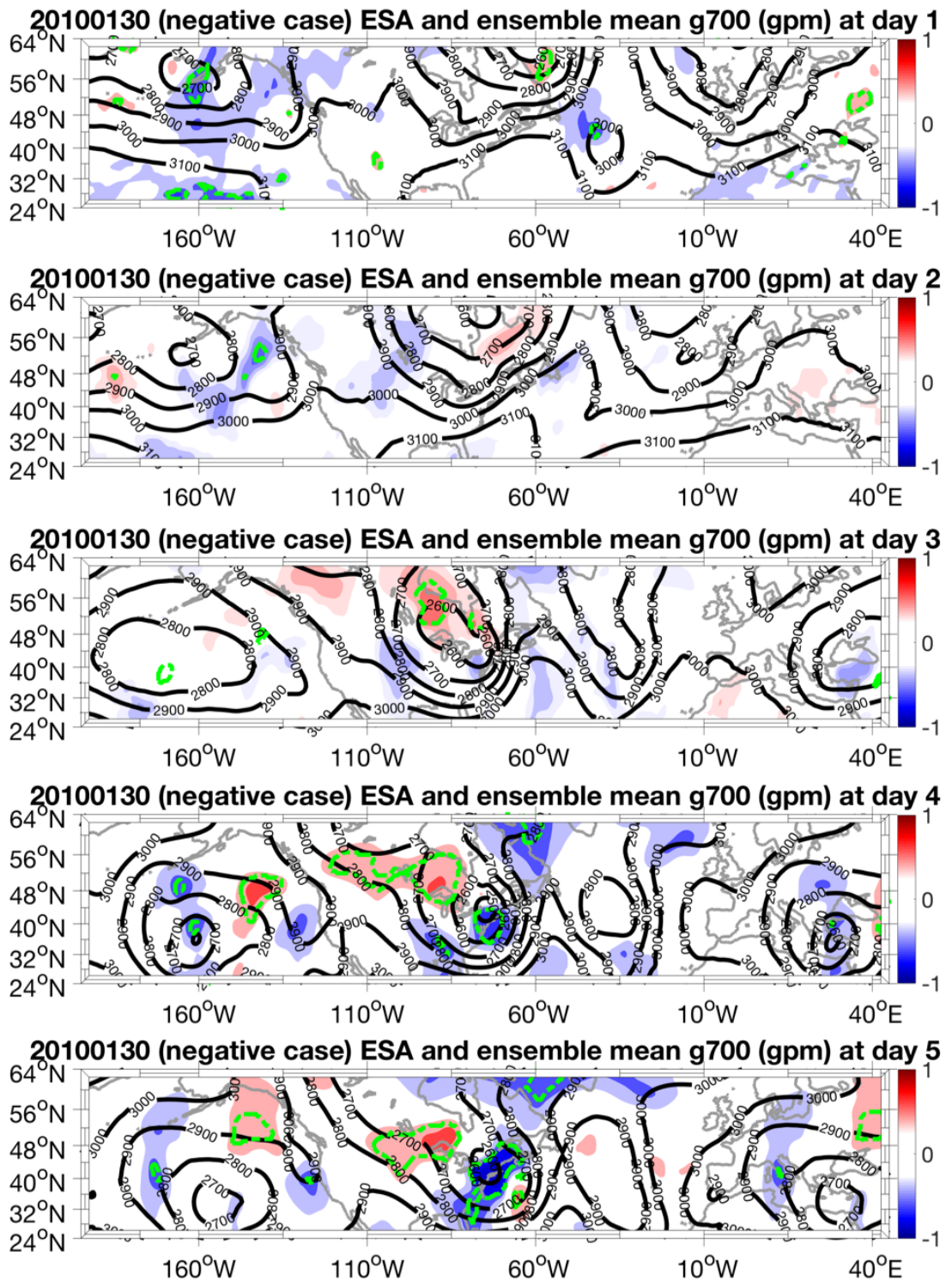


Figure 20. 20100130 (overpredicted case) daily ensemble sensitivity (shades) and ensemble mean geopotential height at 700hPa (contours). The green line area has significance over 95%.

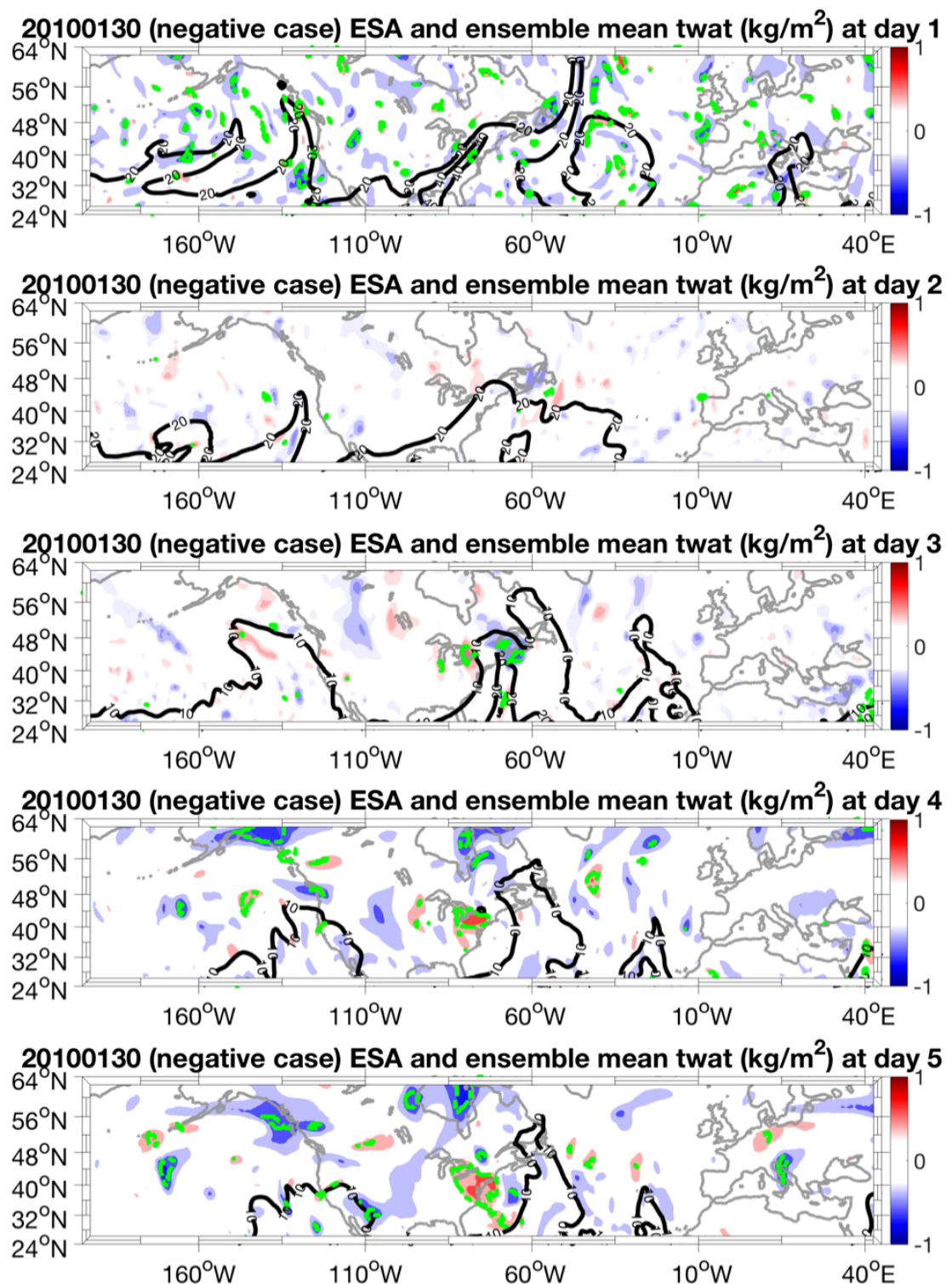


Figure 21. 20100130 (overpredicted case) daily ensemble sensitivity (shades) and ensemble mean total column water (contours). The green line area has significance over 95%.

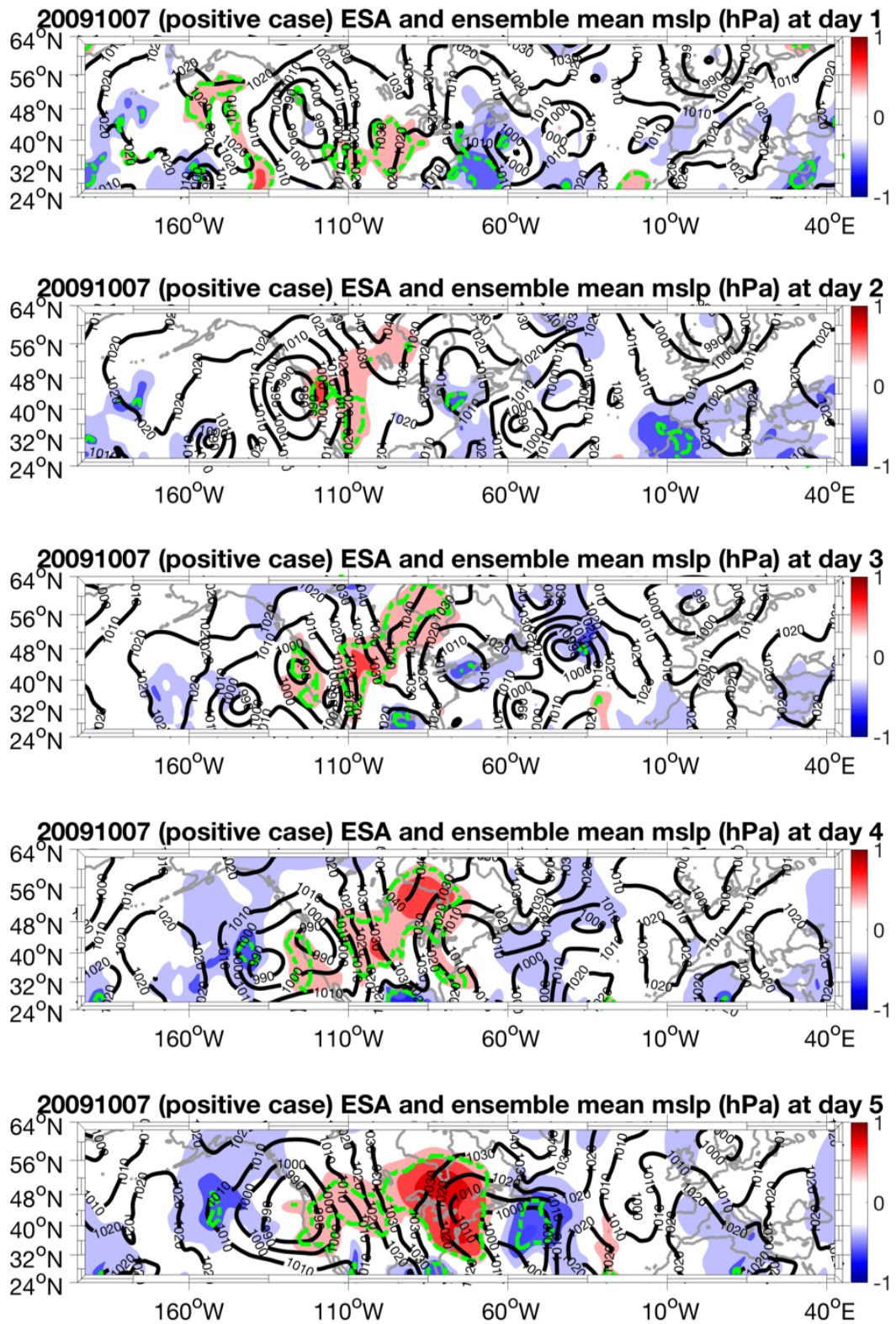


Figure 22. 20091007 (underpredicted case) daily ensemble sensitivity (shades) and ensemble mean mean sea level pressure (contours). The green line area has significance over 95%.

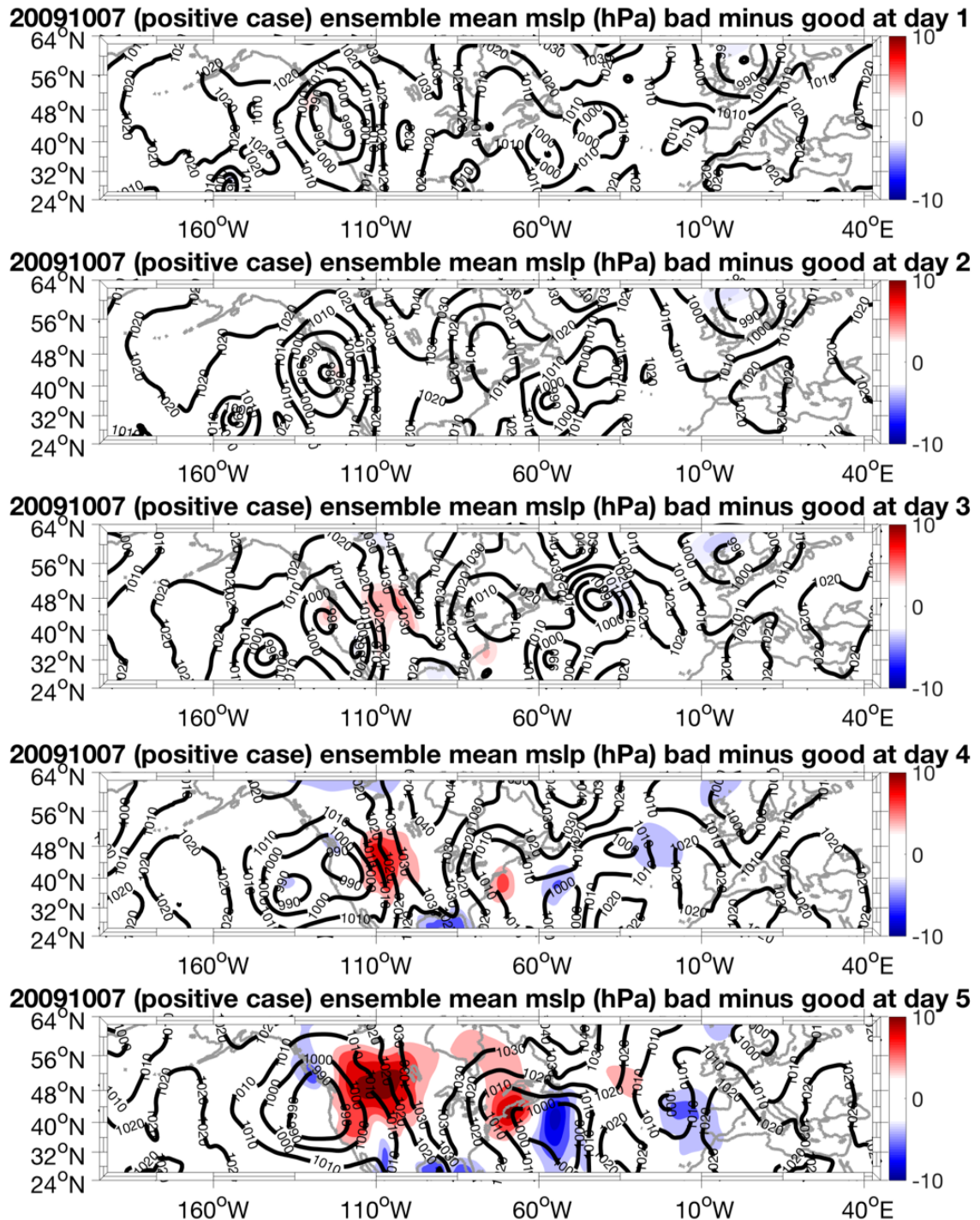


Figure 23. 20091007 (underpredicted case) daily bad member minus good member's difference (shades) and ensemble mean mean sea level pressure (contours).

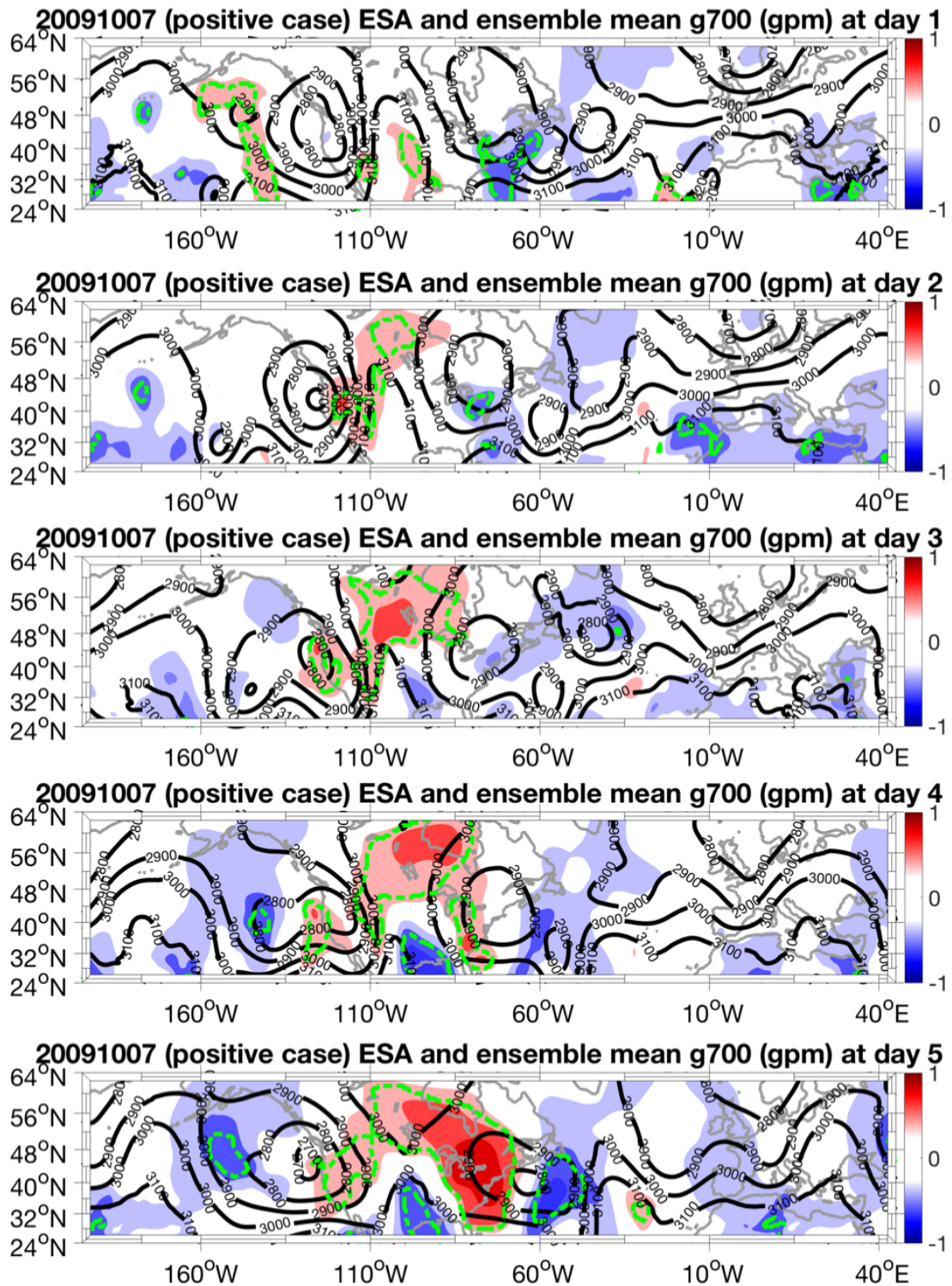


Figure 24. 20091007 (underpredicted case) daily ensemble sensitivity (shades) and ensemble mean geopotential height at 700hPa (contours). The green line area has significance over 95%.

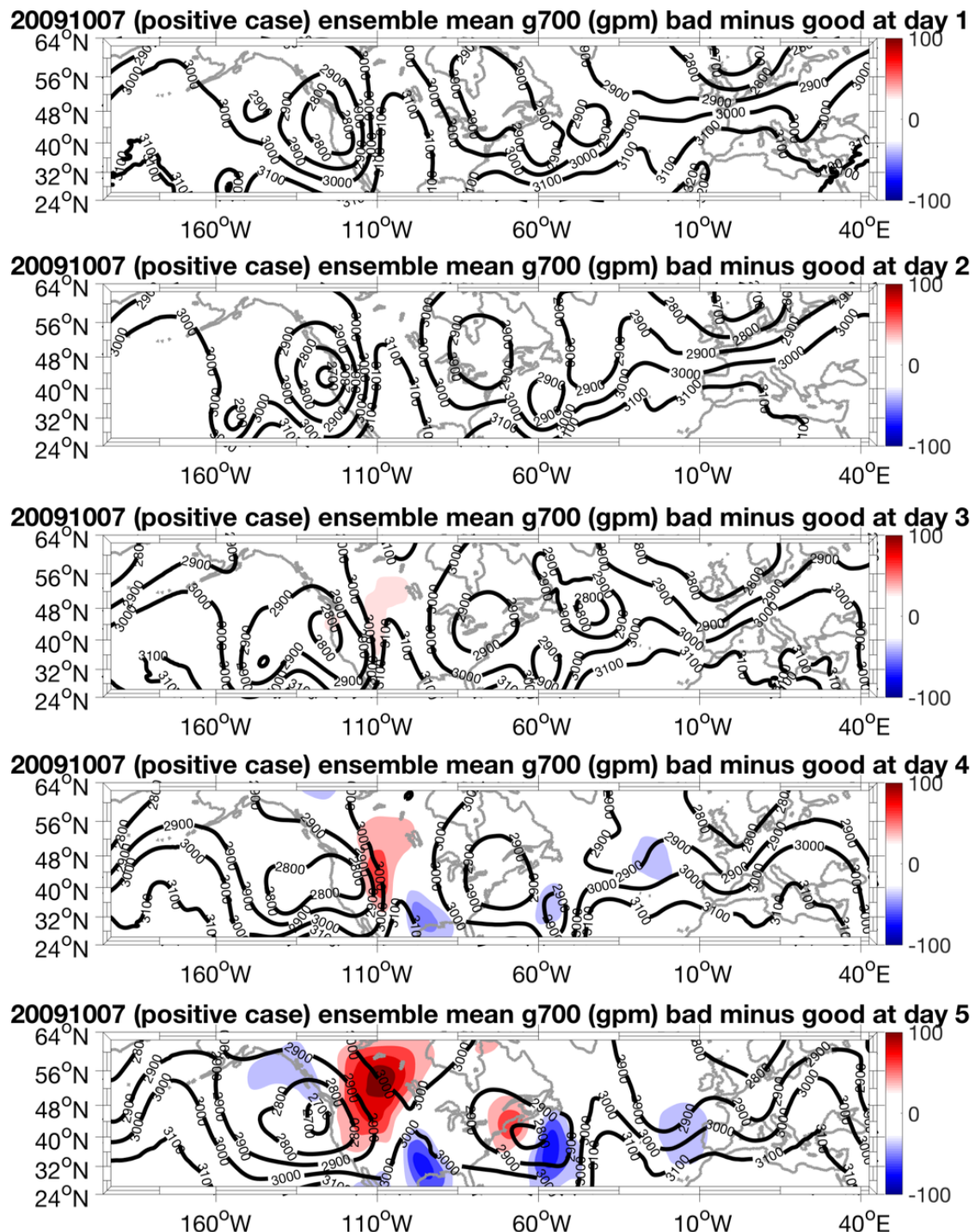


Figure 25. 20091007 (underpredicted case) daily bad member minus good member's difference (shades) and ensemble mean geopotential height at 700 hPa (contours).

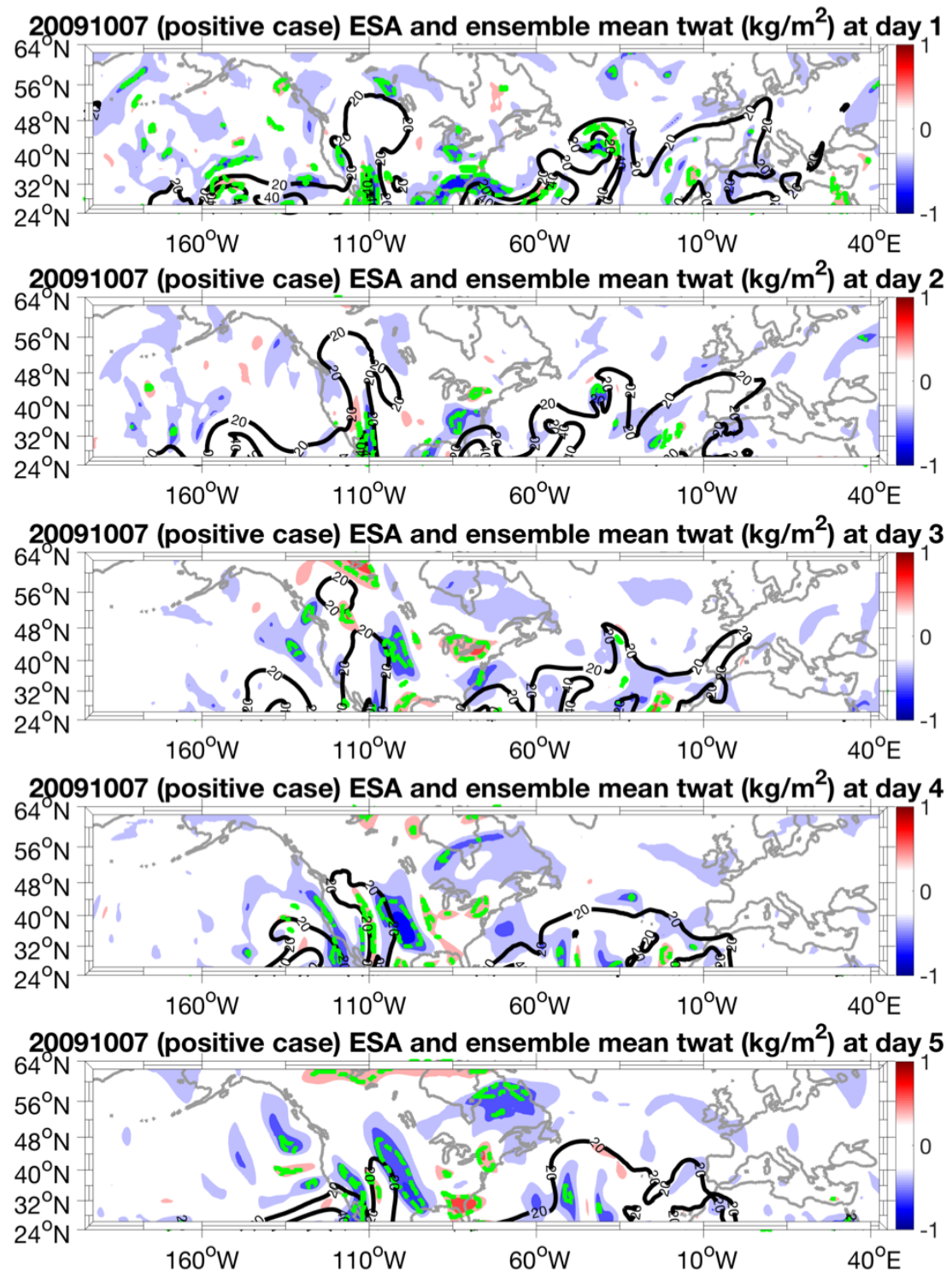


Figure 26. 20091007 (underpredicted case) daily ensemble sensitivity (shades) and ensemble mean total column

water (contours). The green line area has significance over 95%.

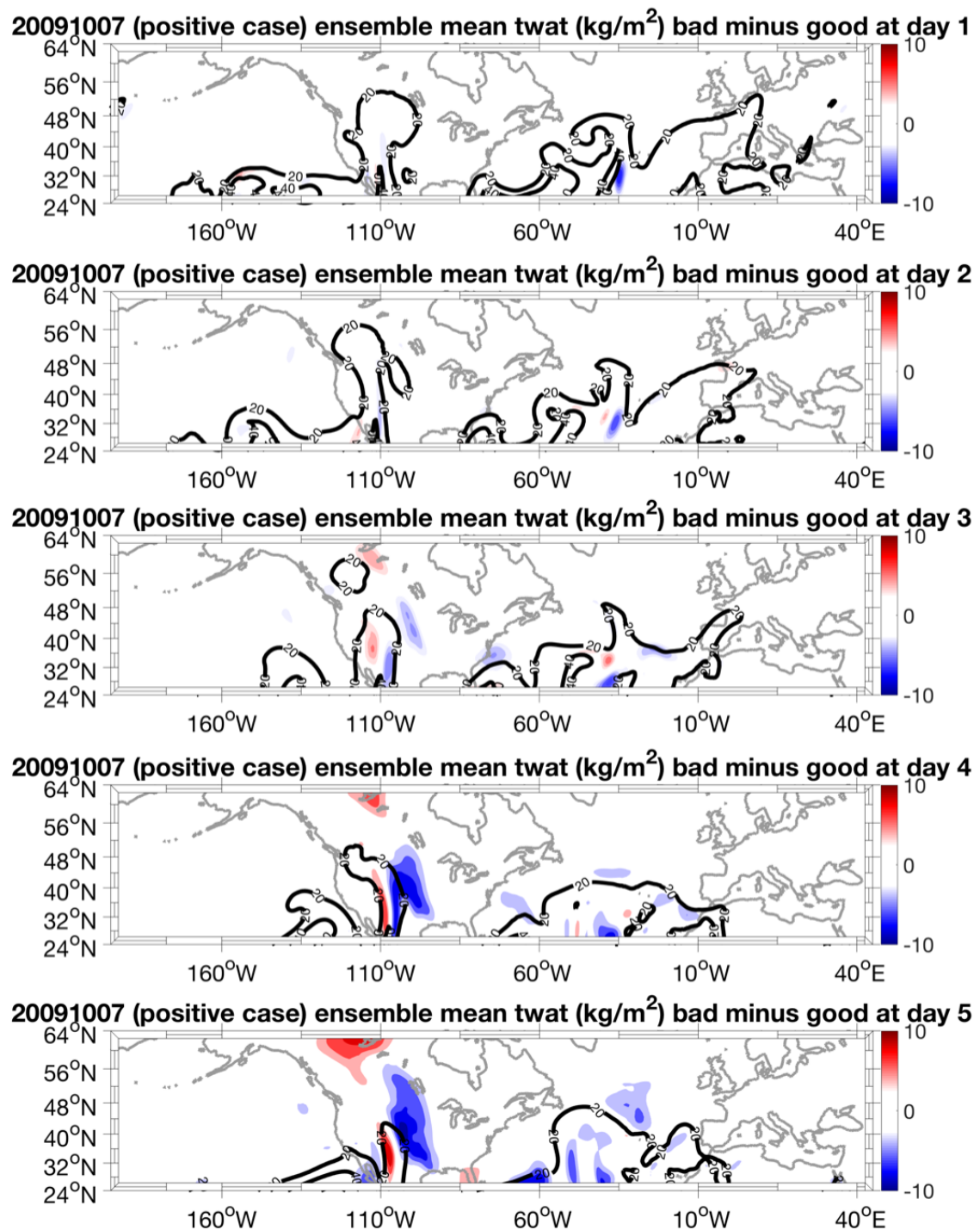


Figure 27. 20091007 (underpredicted case) daily bad member minus good member's difference (shades) and ensemble mean total column water (contours).

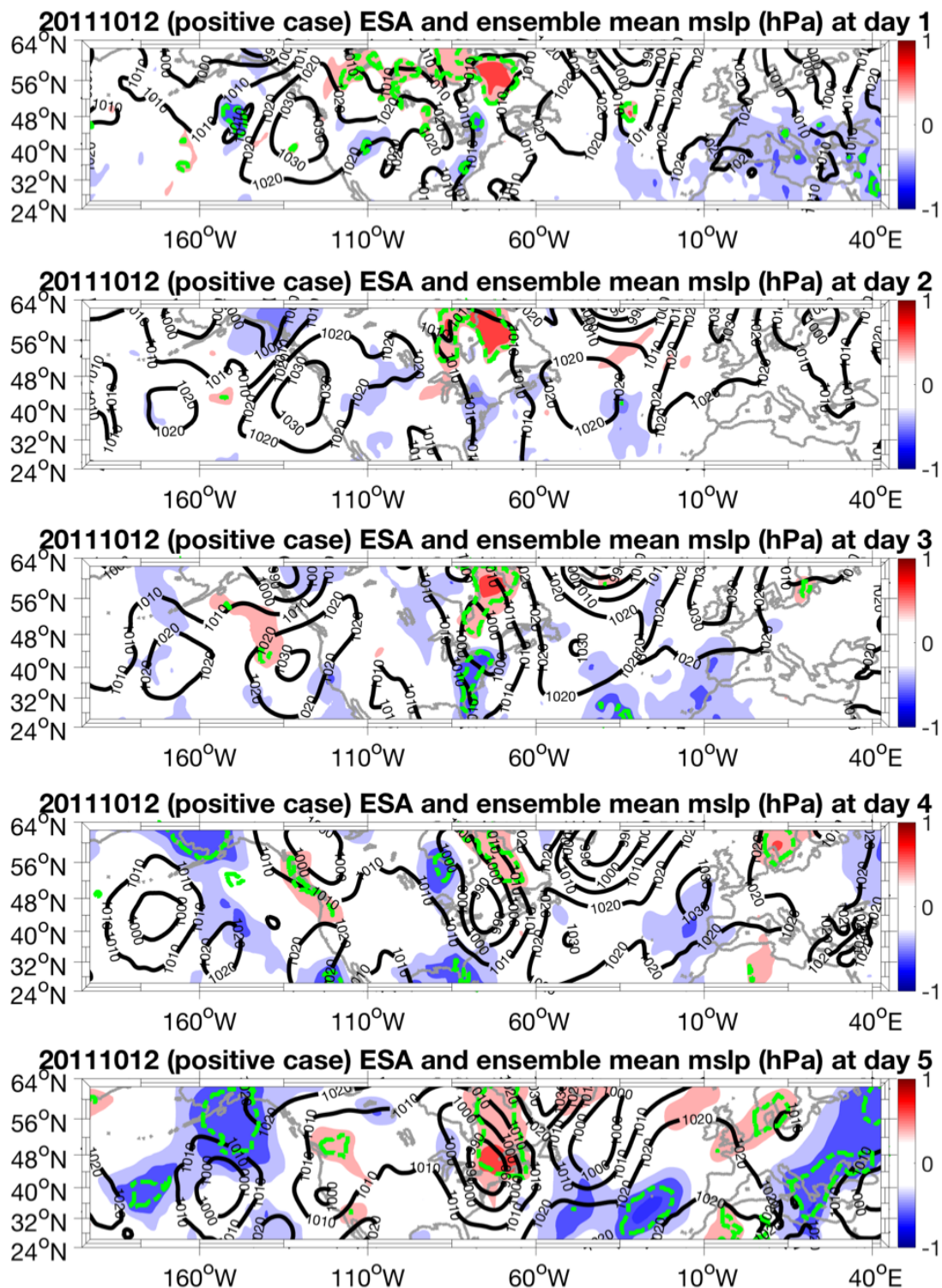


Figure 28. 20111012 (underpredicted case) daily ensemble sensitivity (shades) and ensemble mean mean sea level pressure (contours). The green line area has significance over 95%.

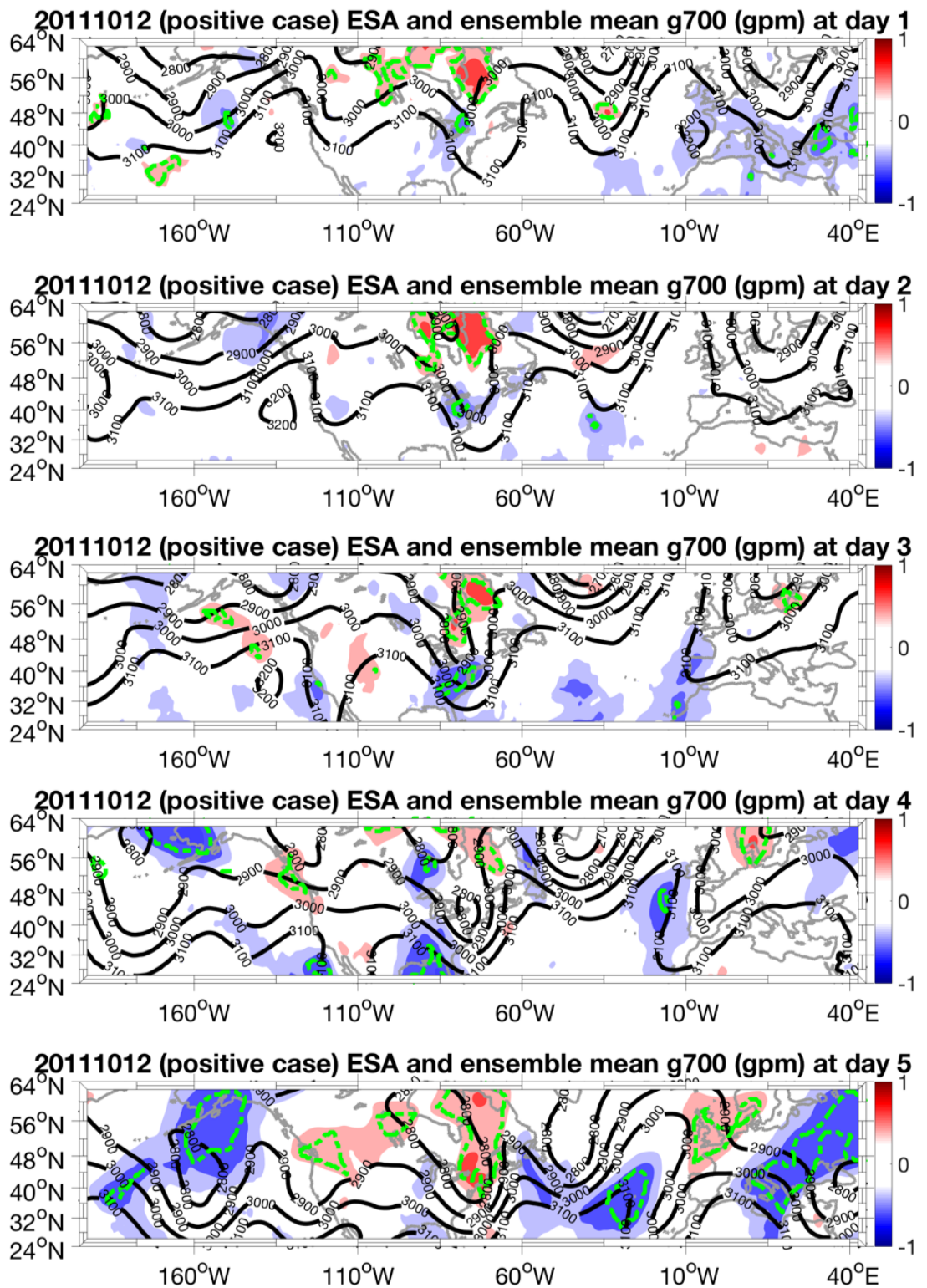


Figure 29. 20111012 (underpredicted case) daily ensemble sensitivity (shades) and ensemble mean geopotential height at 700hPa (contours). The green line area has significance over 95%.

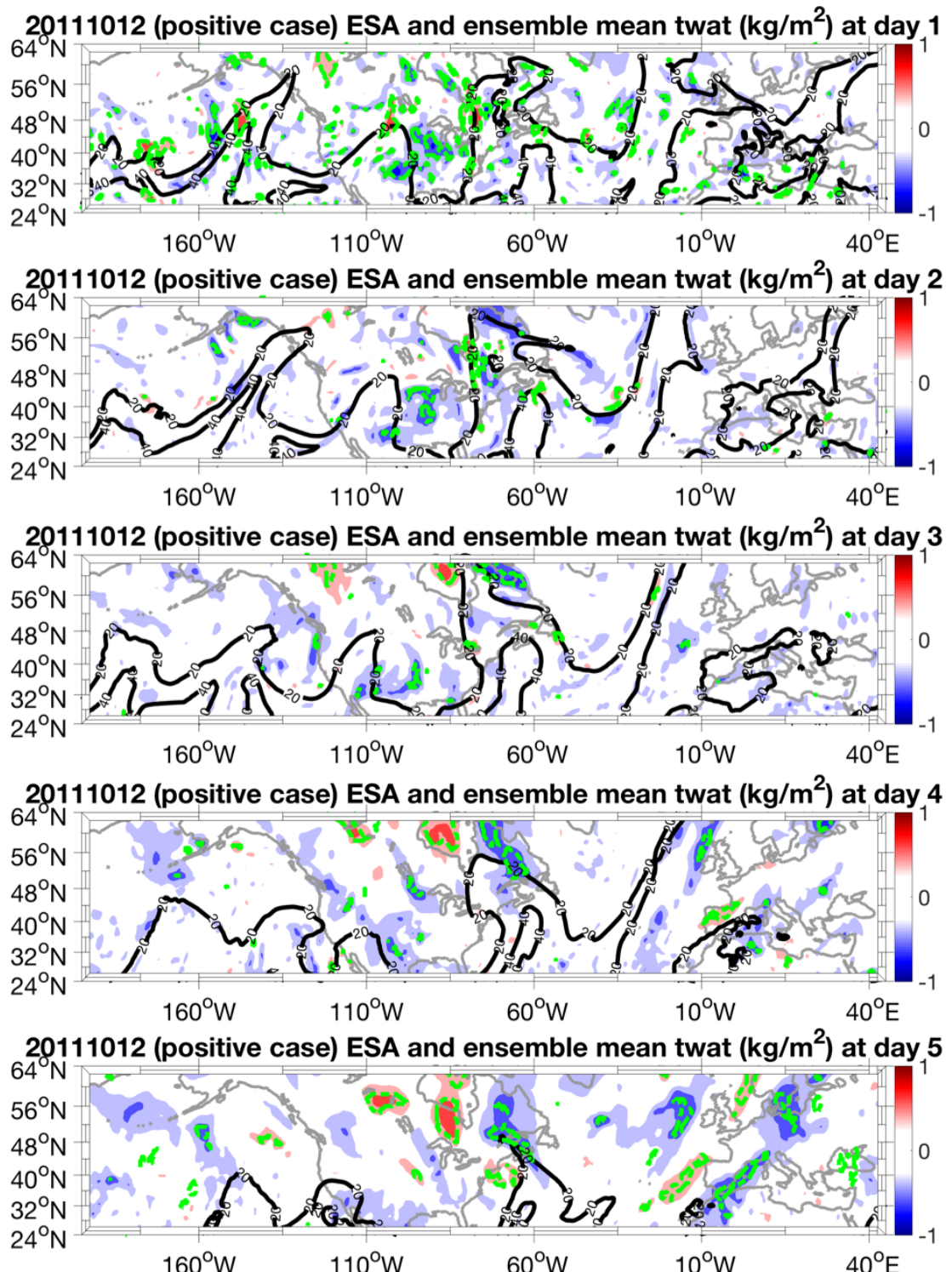


Figure 30. 20111012 (underpredicted case) daily ensemble sensitivity (shades) and ensemble mean total column water (contours). The green line area has significance over 95%.

Chapter V: Conclusion

This research investigated the potential reasons for extratropical cyclone errors in operational models. The control member and ensemble members of the Global Ensemble Forecast System were used in this study. Techniques like cyclone relative approach and ensemble sensitivity analysis are used to help understand the factors associated with the mean sea level pressure cyclone center errors. The overdeepened cyclones were shifted spatially more to the north over the western Atlantic than underdeepened cyclones. The physical ingredient that may lead to cyclogenesis intensity biases could be latent heat and temperature gradient, meaning that both moist and dry dynamics play important roles in cyclogenesis error formations.

Using a cyclone relative approach, the errors were found to grow rapidly from day 4 to day 5. For mean sea level pressure the overdeepened cases have negative errors (model minus observation) and the underdeepened cases have positive errors. The PV at 320K is stronger in model in overdeepened cases than observed and weaker in underdeepened cases. For temperature gradient at 925 hPa, the cold front area has positive errors for overdeepened cases by day 5 and negative errors for underdeepened cases by day 3. There is more

precipitation than observed for the overdeepened cases and less precipitation than observed for underdeepened cases. The positive precipitation error at day 3 for the overdeepened cases suggests that excessive latent heat release may be contributing to cyclogenesis intensity errors. Moreover, there is significant error in the 925 hPa temperature gradient at day 3 around the cyclone in the error differences plot, which suggests that dry dynamics may be contributing to the cyclone pressure as well around day 3.

The ensemble sensitivity analysis using cyclone relative approach shows that the moisture may also be influencing the cyclogenesis error, and that source may come from upstream to the west. The overdeepened case on 30 January 2010 has a correlation pattern with positive correlation to the west of cyclone center and negative correlation on the center of cyclone center for mean sea level pressure and 700 hPa geopotential height. The moisture has a positive correlation around the west area of cyclone center. These signals imply that if the cyclone is predicted to be more northwestward, the error projection coefficient would be smaller and if there is less moisture around the west area of cyclone center, the error projection coefficient would be smaller. It also suggests there is a short wave trough influence from upstream.

For the underpredicted case on 7 October 2009, the correlation has a pattern with positive signal to the west and negative signal to the east of cyclone center for mean sea level pressure and 700 hPa geopotential height. These signal shows that if the cyclone center is predicted to be more west, the error projection coefficient would be smaller. As for the total column water, there is an upstream negative correlation meaning that if the moisture is less in upstream, the error projection coefficient would be larger. The bad minus good members results show similar difference pattern as that of ESA correlation pattern, thus implying that the ESA results are reliable.

For the third underpredicted case on 12 October 2011, the local positive correlation developed from the north, implying that if the local contours for mean sea level pressure or 700 hPa geopotential height is lower (the system gets stronger), the error projection coefficient would be smaller. As for the total column water, there is a positive correlation to the west and a negative correlation to the east. This moisture signal indicates that if the total column water decreases on the west side of cyclone center, the error projection coefficient would decrease and the opposite applies to the east of cyclone center. Overall, the mechanism could be explained in this way: The lower moisture on the warm side of cyclones would lead

to a weaker upper tropospheric latent heat release, and hence a less amplified PV field, and a weaker cyclone. Additionally, a weaker temperature gradient at 925 hPa would also cause a weaker cyclone.

The following suggestions could be attempted for future work. Firstly, conducting a controlled experiment in which Weather Research and Forecasting Model (WRF) is operated to get its own ensembles by only perturbing certain physics tendencies. Secondly, confirm the results using the ECMWF or GEFS reforecast fields to see if the cyclones from these ensembles show the same rates of error growth and if the ECMWF over-deepened cases also have pressure errors at day3 related to any precipitation errors.

References

- Adler, R. F., G. Gu, and G. J. Huffman, 2012: Estimating climatological bias errors for the Global Precipitation Climatology Project (GPCP). *J. Appl. Meteor. Climatol.*, 51, 84–99.
- Bell, R. J., S. L. Gray, and O. P. Jones (2017), North Atlantic storm driving of extreme wave heights in the North Sea, *J. Geophys. Res. Oceans*, 122, 3253–3268.
- Bengtsson, L., K. I. Hodges, and N. Keenlyside, 2009: Will extratropical storms intensify in a warmer climate? *J. Climate*, 22, 2276–2301.
- Buizza, J. Tribbia, F. Molteni, and T. Palmer, 1993: Computation of optimal unstable structures for a numerical weather prediction model. *Tellus*, 45A, 388–407.
- Chagnon, J., S. L. Gray, and J. Methven (2013), Diabatic processes modifying potential vorticity in a North Atlantic cyclone, *Q. J. R. Meteorol. Soc.*, 139, 1270–1282.
- Chang, E. K. M., and S. W. Song, 2006: The seasonal cycles in the distribution of precipitation around cyclones in the western North Pacific and Atlantic. *J. Atmos. Sci.*, 63, 815–839.
- , M. Zheng, and K. Raeder, 2013: Medium-range ensemble sensitivity analysis of two extreme pacific extratropical cyclones. *Mon. Wea. Rev.*, 141, 211–231.
- Charles, M. E., and B. A. Colle, 2009: Verification of extratropical cyclones within the NCEP operational models. Part I: Analysis errors and short-term NAM and GFS forecasts. *Wea. Forecasting*, 24, 1173–1190.
- , and B. A. Colle, 2009: Verification of extratropical cyclones within the NCEP operational models. Part II: The Short-Range Ensemble Forecast system. *Wea. Forecasting*, 24, 1191–1214.

- Colle BA, Buonaiuto F, Bowman MJ, Wilson RE, Flood R, Hunter R, Mintz A, Hill E. 2008. New York City's vulnerability to coastal flooding. *Bull Am Meteorol Soc*. 89:829841.
- , Zhang Z., Lombardo K. A., Chang K. M. , Lui P., and Zhang M., 2013: Historical evaluation and future prediction of eastern North American and western Atlantic extratropical cyclones in the CMIP5 models during the cool season. *J. Climate*, 26, 6882–6903.
- Davies, H. C., and M. Didone, 2013: Diagnosis and dynamics of forecast error growth. *Mon. Wea. Rev.*, 141, 2483–2501.
- Dee, Dick & National Center for Atmospheric Research Staff (Eds). Last modified 04 Aug 2017. "The Climate Data Guide: ERA-Interim." Retrieved from <https://climatedataguide.ucar.edu/climate-data/era-interim>.
- Easterling DR, Meehl J, Parmesan C, Chagnon S, Karl TR, Mearns LO. 2000. Climate extremes: observations, modeling, and impacts. *Science* 289:2068–74.
- Eckhardt, S., A. Stohl, H. Wernli, P. James, C. Forster, and N. Spichtinger, 2004: A 15-year climatology of warm conveyor belts. *J. Climate*, 17, 218–237.
- Epstein, E. S., 1969: Stochastic dynamic prediction. *Tellus*, 21, 739– 759.
- Field, P. R., A. Gettelman, R. B. Neale, R. Wood, P. J. Rasch, and H. Morrison, 2008: Midlatitude cyclone compositing to constrain climate model behavior using satellite observations. *J. Climate*, 21, 5887–5903.
- , and R. Wood, 2007: Precipitation and cloud structure in midlatitude cyclones. *J. Climate*, 20, 233–254.
- Froude, L. S. R., L. Bengtsson, and K. I. Hodges, 2007: The Prediction of Extratropical Storm Tracks by the ECMWF and NCEP Ensemble Prediction Systems. *Mon. Wea. Rev.*, 135, 2545–2567.

Goodwin, L. C. 2003: Weather-Related Crashes on U.S. Highways in 2001. Mitretek System, Inc., for U.S. Department of Transportation, 8pp.

Gray, S.L., C.M. Dunning, J. Methven, G. Masato, and J.M. Chagnon, 2014: Systematic Model Forecast Error in Rossby Wave Structure. *Geophys. Res. Lett.*, 41, 2979–2987.

Grumm, R. H., 2014: Eastern United States snow event of 2-3 February 2014: dealing with uncertainty and short predictability horizons. <http://cms.met.psu.edu/sref/severe/2014/03Feb2014SNOW.pdf>

Hawcroft MK, Shaffrey LC, Hodges KI, Dacre HF (2015) Can climate models represent the precipitation associated with extratropical cyclones? *Clim Dyn* 1–17.

Hodges, K. I., 1994: A general method for tracking analysis and its application to meteorological data. *Mon. Wea. Rev.*, 122, 2573–2586.

Huffman GJ, Adler RF, Arkin PA, Chang A, Ferraro R, Gruber A, Janowiak J, McNab A, Rudolf B, Schneider U. 1997. The Global Precipitation Climatology Project (GPCP) combined precipitation dataset. *Bulletin of the American Meteorological Society* 78(1): 5–20.

Johnson C, Swinbank R. 2009. Medium-range multimodel ensemble combination and calibration. *Q. J. R. Meteorol. Soc.* 135: 777–794.

Karl T.R., Easterling D.R. (1999) Climate Extremes: Selected Review and Future Research Directions. In: Karl T.R., Nicholls N., Ghazi A. (eds) *Weather and Climate Extremes*. Springer, Dordrecht

Korfe, N, G., 2016: Evaluation of Cool-Season Extratropical Cyclones in a Multi-Model Ensemble for Eastern North America and the Western Atlantic Ocean.

- Lamberson, W. S., Torn, R. D., Bosart, L. F., & Magnusson, L., 2016. Diagnosis of the Source and Evolution of Medium-Range Forecast Errors for Extratropical Cyclone Joachim. *Weather and Forecasting*, (2016).
- Leith, C. E., 1974: Theoretical skill of Monte Carlo forecasts. *Mon. Wea. Rev.*, 102, 409–418.
- Lillo SP, Parsons DB. 2016. Investigating the dynamics of error growth in ecmwf medium range forecast
- Lorenz, E. N. (1963). Deterministic nonperiodic flow. *J. Atmos. Sci.*, 20: 130–141.
- . (1982). Atmospheric predictability experiments with a large numerical model. *Tellus*, 34: 505– 513.
- Melhauser, C., and F. Zhang, 2012: Practical and intrinsic predictability of severe and convective weather at the mesoscales. *J. Atmos. Sci.*, 69, 3350–3371.
- Molteni, F., R. Buizza, T. N. Palmer, and T. Petroliagis, 1996: The ECMWF ensemble system: Methodology and validation. *Quart. J. Roy. Meteor. Soc.*, 122, 73–119.
- Naud, C. M., D. J. Posselt, and S. C. van den Heever, 2012: Observational analysis of cloud and precipitation in midlatitude cyclones: Northern versus Southern Hemisphere warm fronts. *J. Climate*, 25, 5135–5151.
- Picca J. C., D. M. Schultz, B. A. Colle, S. Ganetis, D. R. Novak, and M. Sienkiewicz, 2014: The value of dual-polarization radar in diagnosing the complex microphysical evolution of an intense snowband. *Bull. Amer. Meteor. Soc.*
- Rodwell, M. J., and Coauthors, 2013: Characteristics of occasional poor medium-range weather forecasts for Europe. *Bull. Amer. Meteor. Soc.*, 94, 1393–1405.
- Stensrud, D.J., H.E. Brooks, J. Du, M.S. Tracton, and E. Rogers, 1999: Using ensembles for short-range

forecasting. *Mon. Wea. Rev.*, 127, 433–446.

Sun, Y. Q., & Zhang, F. (2016): Intrinsic versus Practical Limits of Atmospheric Predictability and the Significance of the Butterfly Effect. *Journal of the Atmospheric Sciences*, 73(3), 1419–1438.

Torn, R. D., J. S. Whitaker, P. Pegion, T. M. Hamill, and G. J. Hakim, 2015: Diagnosis of the source of GFS medium-range track errors in Hurricane Sandy (2012). *Mon. Wea. Rev.*, 143, 132–152.

Toth, Z., E. Kalnay, S. M. Tracton, R. Wobus, and J. Irwin (1997), A synoptic evaluation of the NCEP ensemble, *Weather Forecast.*, 12, 140–153.

Uccellini, L. W., and Coauthors, 1995: Forecasting the 12–14 March 1993 superstorm. *Bull. Amer. Meteor. Soc.*, 76, 183–199.

Weisman, M. L., and Coauthors, 2015: The Mesoscale Predictability Experiment (MPEX). *Bull. Amer. Meteor. Soc.*, 96, 2127–2149.

Wang, C.-C., and J. C. Rogers, 2001: A composite study of explosive cyclogenesis in different sectors of the North Atlantic. Part I: Cyclone structure and evolution. *Mon. Wea. Rev.*, 129, 1481–1499.

Zhang, F., C. Snyder, and R. Rotunno, 2002: Mesoscale Predictability of the “Surprise” Snowstorm of 24–25 January 2000. *Mon. Wea. Rev.*, 130, 1617–1632.

Zheng, M., E. K. M. Chang, and B. Colle, 2013: Ensemble sensitivity tools for assessing extratropical cyclone intensity and track predictability. *Wea. Forecasting*, 28, 1133–1156.

Zhu, H., and A. Thorpe, 2006: Predictability of extratropical cyclones: The influence of initial condition and model uncertainties. *J. Atmos. Sci.*, 63, 1483–1497.

Zhu, Y., Z. Toth, R. Wobus, D. Richardson, and K. Mylne, 2002: On the economic value of ensemble-based weather forecasts. *Bull. Amer. Meteor. Soc.*, 83, 73–83.